SCHOOL OF GEOSCIENCES

Acoustic wavefield modelling using the Foldy method with application to seismic interferometry

Matlab code user guide with theory and worked examples

Erica Galetti [1], Andrew Curtis [2], David Halliday [3], Dirk-Jan van Manen [4]

5 March 2013

[1]erica.galetti@ed.ac.uk, [2]Andrew.Curtis@ed.ac.uk, [3]dhalliday@slb.com, [4]dmanen@slb.com

Summary

This guide accompanies the Foldy acoustic modelling Matlab code written by Erica Galetti (now at the University of Edinburgh, School of GeoSciences) based on similar codes written by David Halliday and Dirk-Jan van Manen (now at Schlumberger Gould Research - SGR).

The code uses the Foldy method to model the direct and scattered acoustic wavefield from one (or more) sources to one (or more) receivers. Unlike other modelling schemes such as finite-differences, the Foldy method is a pseudo-analytic method of waveform modelling which allows a theoretically exact construction of the direct and scattered parts of a wavefield. Its main advantage lies in the fact that, while all multiple scattering interactions are taken into account, numerical dispersion errors are avoided, making it an ideal modelling method to test new theory in seismology and in seismic interferometry in particular.

Whithin this guide, the theory behind the modelling code is presented, followed by a detailed description of interferometric theory in the inter-receiver (van Manen et al. (2005) and Wapenaar & Fokkema (2006)), inter-source (Curtis et al. (2009)) and source-receiver (Curtis & Halliday (2010)) case. A number of modelling and interferometry examples which are included in the package are also presented.

Contents

CHAPTER 1

Quick-Start Guide

1.1 Using the Modelling Code

1.1.1 Code Description[1]

The Foldy acoustic modelling code `model_gfs_p_scat_acoust.m` is a well commented Matlab script that models direct and scattered wavefields generated by monopole and dipole sources of volume injection and volume injection rate, recorded by monopole and dipole receivers. The code uses the analytical Green's function formulae in Appendix A.1 to compute the impulse response of a medium of constant velocity c, with the option of applying a Ricker wavelet of a certain central frequency as source signature. In the absence of scatterers, the impulse response is evaluated only using the Green's function formulae in Appendix A.1; when scatterers are present, the code uses the theory of multiple scattering (section 2.1) developed by Foldy (1945) to compute the scattered part of the wavefield.

The code consists of a main Matlab function and a number of sub-functions that work in combination:

- `model_gfs_p_scat_acoust.m`: the main modelling function, models direct and scattered acoustic pressure Green's functions in a homogeneous acoustic medium in the frequency domain, by applying the equations listed in Appendix A.1.
- `acoustic_p_gfs_direct_f.m`: models direct Green's functions in a homogeneous acoustic medium in the frequency domain. These Green's functions are fed into `model_gfs_p_scat_acoust.m` to evaluate the total wavefield through the medium.
- `rickerwavl_time.m`: computes a Ricker wavelet of any desired central frequency

[1] This section is an (adapted) excerpt from Galetti et al. (2013).

over a certain time interval. The length of the wavelet is given by `ceil(1/(fc*dt))*dt`, where `fc` is the central frequency of the wavelet and `dt` is the sampling interval, given by `1/(2*maxf)`, with `maxf` equal to the maximum modelled frequency.

- `centerfreqs.m`: creates a centred frequency spectrum from the one-sided spectrum obtained from modelling.

The outputs can be given in either or both of the frequency and time domains. If scattering is included, the wavefields are given as the sum of the direct and scattered wavefields (total wavefield), with the option of including separate direct and/or scattered wavefields in the output. Standard output includes a vector of the actual frequency/time samples for which output values are given, and the actual Ricker wavelet used if a source wavelet is applied.

In addition to the core modelling functions, the code package includes the following functions to perform interferometry and plotting:

- `do_xcorr_int.m`: performs either inter-receiver or inter-source cross-correlational interferometry in the time or frequency domain.
- `makecircbound.m`: creates a circular boundary of evenly-spaced points.
- `wiggles.m`: creates a wiggle plot of seismic traces (as used in the worked example in section 2.3.3: `example_3__inter_receiver_F_array.m`).

1.1.2 Input/Output

The function call reads as follows:

```
[varargout] = model_gfs_p_scat_acoust (srx, rxs, maxfreq, nfreq, c, dim, ...
    srctype, diploc, scatflag, wavlflag, freqflag, timeflag, sepflag, ...
    varargin)
```

In the input:

`srx` location of sources in matrix having:

1st column	x-coords
2nd column	y-coords (ignored by code if `dim` set to `'1d'`)
3rd column	z-coords (ignored by code if `dim` set to `'1d'`, `'2d'` or `'2d_far'`)

`rcx` location of receivers in matrix having:

- 1st column: x-coords
- 2nd column: y-coords (ignored by code if `dim` set to `'1d'`)
- 3rd column: z-coords (ignored by code if `dim` set to `'1d'`, `'2d'` or `'2d_far'`)

`maxfreq` maximum frequency to model

`nfreq` number of frequencies to model (the code rounds this up to the nearest power of two to make `fft`/`ifft` run faster - go to lines 277-278 to change this)

`c` velocity of the medium (in m s^{-1})

`dim` number of dimensions - important for geometrical spreading

- `'1d'` uses the 1D Green's function formula (equation (A.2))
- `'2d'` uses the exact 2D Green's function formula (equation (A.3))
- `'2d_far'` uses the far-field 2D Green's function formula (equation (A.4))
- `'3d'` uses the 3D Green's function formula (equation (A.5))

`srctype` select source type:

- `'volinjpos'` positive volume injection (equations (2.11) and (A.15))
- `'volinjneg'` negative volume injection (equations (2.16) and (A.17))
- `'volinjratepos'` positive volume injection rate (equations (2.21) and (A.16))
- `'volinjrateneg'` negative volume injection rate (equations (2.26) and (A.18))

`diploc` compute the dipole (derivative) Green's function...

`'srcdip'`	...with respect to sources (as in inter-receiver interferometry)
`'recdip'`	...with respect to receivers (as in inter-source interferometry)

`scatflag` are there any scatterers?

`'scatn'`	no
`'scaty'`	yes

`wavlflag` apply source wavelet?

`'wavln'`	no
`'wavly_pos'`	yes, with Ricker wavelet at positive times
`'wavly_centr'`	yes, with Ricker wavelet centred on zero time
`'wavly_neg'`	yes, with Ricker wavelet at negative times
`'wavly_shift'`	yes, with Ricker wavelet shifted by `ts` seconds from zero

`freqflag` output in frequency domain?

`'freqn'`	no frequency-domain output
`'freqy_1nf'`	output frequencies in range `[1:nf]` (zero not included)
`'freqy_1s'`	output positive frequency spectrum in range `[0:nf]` (zero included)
`'freqy_2s'`	output double-sided frequency spectrum in range `[-nf:nf-1]`

`timeflag` output in time domain?

`'timen'`	no time-domain output
`'timey'`	output wavefields in time domain

`sepflag` separate direct and scattered wavefield in distinct outputs?

`'tot'`	output total (sum of direct and scattered)
`'dir'`	output total and direct
`'scat'`	output total and scattered
`'dirscat'`	output total, direct and scattered

`Varargin` includes:

`scats`	location of scatterers in matrix having:	
	1st column	x-coords
	2nd column	y-coords (ignored by code if `dim` set to `'1d'`)
	3rd column	z-coords (ignored by code if `dim` set to `'1d'`, `'2d'` or `'2d_far'`)
	4th+ column	imaginary part of scattering amplitude [2]
`fc`	central frequency of Ricker wavelet	
`ts`	time-shift (in s) of peak of Ricker wavelet (only needed if `wavlflag` is set to `'wavly_shift'`; gets rounded up to `ceil((1/fc)/dt)*dt` by the code)	

When `'wavly_shift'` is selected, the central frequency `fc` and the time-shift `ts` should be inserted in the function call as an array (`[fc,ts]`).

In the output (`varargout`):

`frequencies`	frequency vector matching the modelled frequencies
`gf_mon_p_f`	monopole source/receiver, total wavefield, frequency domain
`gf_dip_p_f`	dipole source/receiver, total wavefield, frequency domain
`gfdir_mon_p_f`	monopole source/receiver, direct wavefield, frequency domain
`gfdir_dip_p_f`	dipole source/receiver, direct wavefield, frequency domain
`gfscat_mon_p_f`	monopole source/receiver, scattered wavefield, frequency domain
`gfscat_dip_p_f`	dipole source/receiver, scattered wavefield, frequency domain
`time`	time vector matching the time domain outputs
`gf_mon_p_t`	monopole source/receiver, total wavefield, time domain
`gf_dip_p_t`	dipole source/receiver, total wavefield, time domain
`gfdir_mon_p_t`	monopole source/receiver, direct wavefield, time domain
`gfdir_dip_p_t`	dipole source/receiver, direct wavefield, time domain
`gfscat_mon_p_t`	monopole source/receiver, scattered wavefield, time domain

[2] A detailed discussion on the scattering amplitude A is given in Appendix A.2. As shown in equation (A.13), the imaginary part of the scattering amplitude may or may not depend on frequency.

If $\Im(A)$ is chosen to be independent of frequency, the value of $\Im(A)$ for each scatterer should be entered in the 4th column of `scats`. In this case, the value of $\Im(A)$ should be between $-2*$`min(k)` and 0 in 1D, between -4 and 0 in 2D, and between $-4\pi/$`max(k)` and 0 in 3D, where `k` is the array of wave numbers (`k=2*pi*frequencies/c`).

If $\Im(A)$ is chosen to be dependent on frequency, the values of $\Im(A)$ for each scatterer should be entered as rows from column `4` to column `3+nfreq` of matrix `scats`, with frequency increasing along dimension 2 of the matrix (i.e. first frequency greater than 0 in column `4`, `maxfreq` in column `3+nfreq`).

`gfscat_dip_p_t`	dipole source/receiver, scattered wavefield, time domain
`wavelet_f`	source wavelet in frequency domain
`wavelet_t`	source wavelet in time domain (the centred wavelet has positive time in sample range `[1:nf]`, reverse negative time in sample range `[nf+1:2*nf]`)

Outputs in the frequency domain are given before outputs in the time domain, total wavefields are given before separate wavefields, direct wavefields are given before scattered wavefields. The source wavelets are given at the end of the output in both the frequency and time domain. If the number of inputs and outputs does not match the number of inputs/outputs required for a certain combination of flags, the code stops executing and an error message is given.

1.2 Examples

1.2.1 Input/Output Examples

First, take the maximum frequency to model to be 100 Hz, model 256 frequencies, set the medium velocity to 1000 m s^{-1}, and use positive volume injection sources. Output the total wavefield emitted by monopole and dipole sources `srx` with zero-phase source wavelet of central frequency 30 Hz, scattered by scatterers at `scats`, recorded by receivers at `rxs`, using the far-field two-dimensional Green's function formula, in the frequency domain only from frequency sample 1 to frequency sample 256:

```
[frequencies, gf_mon_p_f, gf_dip_p_f, wavelet_f] = ...
    model_gfs_p_scat_acoust (srx, rxs, 100, 256, 1000, '2d', ...
    'volinjpos', 'srcdip', 'scaty', 'wavly_centr', 'freqy_1nf', 'timen', ...
    'tot', scats, 30)
```

Same as above but also convert the total wavefields to time domain:

```
[frequencies, gf_mon_p_f, gf_dip_p_f, time, gf_mon_p_t, gf_dip_p_t, ...
    wavelet_f, wavelet_t] = model_gfs_p_scat_acoust (srx, rxs, 100, 256, ...
    1000, '2d', 'volinjpos', 'srcdip', 'scaty', 'wavly_centr', ...
    'freqy_1nf', 'timey', 'tot', scats, 30)
```

Same as above but also output the separate direct and scattered wavefields in the frequency and time domain:

```
[frequencies, gf_mon_p_f, gf_dip_p_f, gfdir_mon_p_f, gfdir_dip_p_f, ...
    gfscat_mon_p_f, gfscat_dip_p_f, time, gf_mon_p_t, gf_dip_p_t, ...
    gfdir_mon_p_t, gfdir_dip_p_t, gfscat_mon_p_t, gfscat_dip_p_t, ...
    wavelet_f, wavelet_t] = model_gfs_p_scat_acoust (srx, rxs, 100, 256, ...
```

```
    1000, '2d', 'volinjpos', 'srcdip', 'scaty', 'wavly_centr', ...
    'freqy_1nf', 'timey', 'dirscat', scats, 30)
```

Same as the second example above but with no scattering and with a Ricker wavelet shifted by +0.05 s:

```
[frequencies, gf_mon_p_f, gf_dip_p_f, time, gf_mon_p_t, gf_dip_p_t, ...
    wavelet_f, wavelet_t] = model_gfs_p_scat_acoust (srx, rxs, 100, 256, ...
    1000, '2d', 'volinjpos', 'srcdip', 'scatn', 'wavly_shift', ...
    'freqy_1nf', 'timey', 'tot', [30,0.05])
```

Same as previous but with no source wavelet applied (i.e. just a delta function used):

```
[frequencies, gf_mon_p_f, gf_dip_p_f, time, gf_mon_p_t, gf_dip_p_t] = ...
    model_gfs_p_scat_acoust (srx, rxs, 100, 256, 1000, '2d', ...
    'volinjpos', 'srcdip', 'scatn', 'wavln', 'freqy_1nf', 'timey', 'tot')
```

Same as previous but calculate the Green's functions derivatives at the receivers and only output results in time domain:

```
[time, gf_mon_p_t, gf_dip_p_t] = model_gfs_p_scat_acoust (srx, rxs, 100, ...
    256, 1000, '2d', 'volinjpos', 'recdip', 'scatn', 'wavln', 'freqn', ...
    'timey', 'tot')
```

1.2.2 Example Plots

The waveforms `gf_mon_p_t` shown in Fig. 1.1(a) are obtained by executing the following commands in Matlab:

```
srx = [0,0,0];                          % Source position
rxs = [500,80,0];                       % Receiver position
maxfreq = 100;                          % Maximum frequency to model
nf = 256;                               % Number of frequencies to model
c = 1000;                               % Medium velocity
fc = 30;                                % Central frequency of Ricker wavelet

% Model the wavefield
[time, gf_mon_p_t, gf_dip_p_t, wavelet_t] = model_gfs_p_scat_acoust ...
    (srx, rxs, maxfreq, nf, c, '2d', 'volinjpos', 'srcdip', 'scatn', ...
    'wavly_centr', 'freqn', 'timey', 'tot', fc);

% fftshift source wavelet to center on zero-time (for plotting)
wavelet_t = fftshift(wavelet_t,1);
```

The waveforms in Fig. 1.1(b) are obtained by executing the following commands in Matlab:

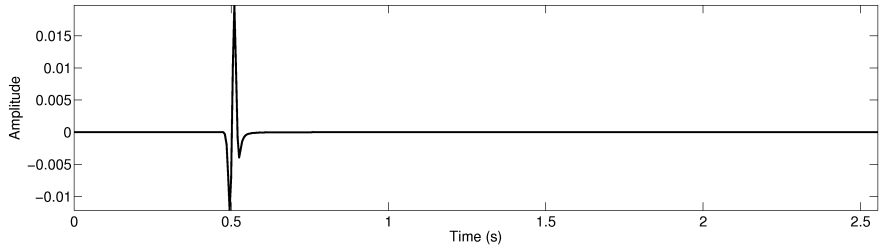

(a)

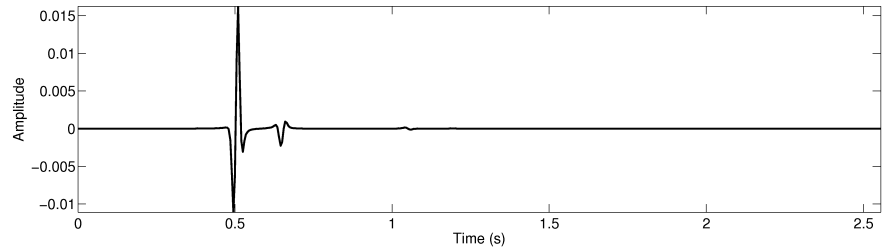

(b)

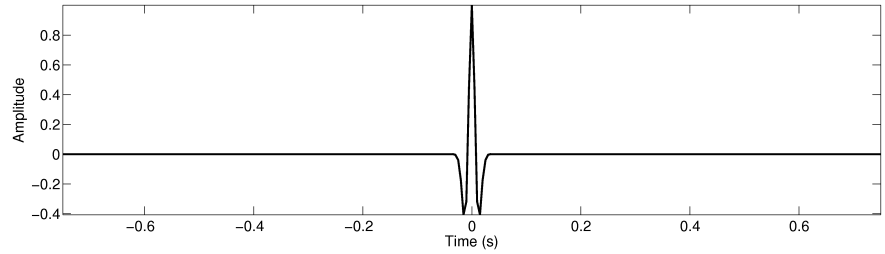

(c)

Figure 1.1. (a) and (b) Wavefields (pressure Green's functions for a monopole source - `gf_mon_p_t`) modelled as indicated in section 1.2.2. (c) Zero-phase source wavelet `wavelet_t` with central frequency 30 Hz, obtained as indicated in section 1.2.2.

```
srx = [0,0,0];                          % Source position
rxs = [500,80,0];                       % Receiver position
scats = [80,-150,0,-3;300,10,0,-4]; % Scatterers position
maxfreq = 100;                          % Maximum frequency to model
nf = 256;                               % Number of frequencies to model
c = 1000;                               % Medium velocity
fc = 30;                                % Central frequency of Ricker wavelet

% Model the wavefield
[time, gf_mon_p_t, gf_dip_p_t, wavelet_t] = model_gfs_p_scat_acoust ...
    (srx, rxs, maxfreq, nf, c, '2d', 'volinjpos', 'srcdip', 'scaty', ...
    'wavly_centr', 'freqn', 'timey', 'tot', scats, fc);

% fftshift source wavelet to center on zero-time (for plotting)
wavelet_t = fftshift(wavelet_t,1);
```

CHAPTER 2

Theory and Applications

2.1 The Foldy Method[1]

Consider a source and a receiver respectively located at position $\mathbf{x}_S$ and $\mathbf{x}_R$ within a homogeneous medium containing a distribution of N scatterers. The total wavefield $\Psi(\mathbf{x}_R)$ recorded at $\mathbf{x}_R$ from the source at $\mathbf{x}_S$ is given by the sum of the direct and scattered wavefield: while the former can easily be calculated as a Green's function from the source to the receiver, the computation of the latter is more complicated as it requires the evaluation of the direct wavefield to each scatterer, wavefield scattering or diffraction, and all possible multiple-scattering interactions of that scattered field. Together these provide the total wavefield radiated by each single scatterer (Figure 2.1). The total wavefield reaching the receiver is finally obtained by summing the components of the wavefield radiated by each scatterer which then propagate to the receiver location.

By assuming the diffractors are limited to isotropic point scatterers we can reduce the multiple scattering process to a system of linear equations which can be solved numerically (Foldy, 1945; Groenenboom & Snieder, 1995). In the frequency domain, the total wavefield $\Psi(\mathbf{x}_R)$ can be expressed as follows:

$$\Psi(\mathbf{x}_R) = \Psi_0(\mathbf{x}_R) + \sum_{i=1}^{N} \Psi(\mathbf{x}^{(i)}) A^{(i)} G(\mathbf{x}_R, \mathbf{x}^{(i)}) \; . \tag{2.1}$$

Here $\Psi_0(\mathbf{x}_R)$ denotes the direct wavefield from $\mathbf{x}_S$ to $\mathbf{x}_R$, $\Psi(\mathbf{x}^{(i)})$ denotes the total wavefield (direct and scattered) reaching scatterer (i) located at $\mathbf{x}^{(i)}$, $A^{(i)}$ is the scattering amplitude of scatterer (i), and $G(\mathbf{x}_R, \mathbf{x}^{(i)})$ is the full Green's function between scatterer (i) and receiver $\mathbf{x}_R$.

[1] This section is an (adapted) excerpt from Galetti et al. (2013).

Also, when the wavefield emitted by the source at $\mathbf{x}_S$ is simply a Green's function convolved with a source wavelet $s(\omega)$, the direct wavefield $\Psi_0(\mathbf{x}_R)$ can be expressed as

$$\Psi_0(\mathbf{x}_R) = s(\omega)G(\mathbf{x}_R, \mathbf{x}_S) \ , \tag{2.2}$$

where $G(\mathbf{x}_R, \mathbf{x}_S)$ denotes the full Green's function between source $\mathbf{x}_S$ and receiver $\mathbf{x}_R$.

The scattering amplitude A is a complex number whose real and imaginary components can be determined from the optical theorem following principles of energy conservation. Within our code, we assume energy loss within the medium is only due to the scattering process and ignore the effects of anelastic attenuation. In order to satisfy the requirement of energy conservation, the real and imaginary parts of A are intimately related, and the value of the imaginary component must fall within a specific range - a detailed discussion on this topic is given in Appendix A.2.

The sum in equation (2.1) essentially means that any scattered wave arriving at $\mathbf{x}_R$ must have come from one of the N scatterers; hence it must have arrived at the scatterer ($\Psi(\mathbf{x}^{(i)})$), been scattered (amplitude and phase scaled by $A^{(i)}$), and must then have propagated to the receiver ($G(\mathbf{x}_R, \mathbf{x}^{(i)})$). The entire series of multiple scattering interactions is therefore included intrinsically within term $\Psi(\mathbf{x}^{(i)})$.

By the same reasoning, the total wavefield $\Psi(\mathbf{x}^{(i)})$ reaching scatterer (i) can be expressed as the sum of the direct and scattered wavefield, where the latter must have been scattered from any and all of the *other* scatterers:

$$\Psi(\mathbf{x}^{(i)}) = \Psi_0(\mathbf{x}^{(i)}) + \sum_{\substack{j=1 \\ j\neq i}}^{N} \Psi(\mathbf{x}^{(j)}) A^{(j)} G(\mathbf{x}^{(i)}, \mathbf{x}^{(j)}) \ , \tag{2.3}$$

where $\Psi_0(\mathbf{x}^{(i)})$ is the direct wavefield from $\mathbf{x}_S$ to scatterer (i), $\Psi(\mathbf{x}^{(j)})$ denotes the total wavefield reaching scatterer (j) located at $\mathbf{x}^{(j)}$, $A^{(j)}$ is the scattering amplitude of scatterer (j), and $G(\mathbf{x}^{(i)}, \mathbf{x}^{(j)})$ is the full Green's function between $\mathbf{x}^{(j)}$ and $\mathbf{x}^{(i)}$.

By swapping the order of terms, expressing the wavefields $\Psi(\mathbf{x}^{(i)})$ and $\Psi_0(\mathbf{x}^{(i)})$ as vectors, and arranging the terms $A^{(j)}G(\mathbf{x}^{(i)}, \mathbf{x}^{(j)})$ into a square matrix of dimension equal to the number of scatterers, equation (2.3) can be re-written as

$$\begin{pmatrix} \Psi_0(\mathbf{x}^{(1)}) \\ \Psi_0(\mathbf{x}^{(2)}) \\ \dots \\ \Psi_0(\mathbf{x}^{(N)}) \end{pmatrix}$$

$$= - \begin{pmatrix} -1 & A^{(2)}G(\mathbf{x}^{(1)}, \mathbf{x}^{(2)}) & \dots & A^{(N)}G(\mathbf{x}^{(1)}, \mathbf{x}^{(N)}) \\ A^{(1)}G(\mathbf{x}^{(2)}, \mathbf{x}^{(1)}) & -1 & \dots & A^{(N)}G(\mathbf{x}^{(2)}, \mathbf{x}^{(N)}) \\ \dots & \dots & \dots & \dots \\ A^{(1)}G(\mathbf{x}^{(N)}, \mathbf{x}^{(1)}) & A^{(2)}G(\mathbf{x}^{(N)}, \mathbf{x}^{(2)}) & \dots & -1 \end{pmatrix} \begin{pmatrix} \Psi(\mathbf{x}^{(1)}) \\ \Psi(\mathbf{x}^{(2)}) \\ \dots \\ \Psi(\mathbf{x}^{(N)}) \end{pmatrix} \ , \tag{2.4}$$

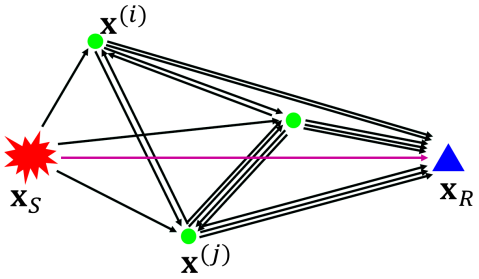

Figure 2.1. The total wavefield reaching a receiver at $\mathbf{x}_R$ from a source at $\mathbf{x}_S$, and scattered by a number of diffractors (e.g. $\mathbf{x}^{(i)}$, $\mathbf{x}^{(j)}$), is given by the sum of a direct term (purple arrow) and a multiply scattered term (sum of all of the black arrows), as indicated in equation (2.1).

where the term on the left-hand side is defined to be a vector $\mathbf{\Psi_0}$ containing the direct wavefields from the source at $\mathbf{x}_S$ to each scatterer, the first term on the right-hand side is matrix $\mathbf{M}$ containing the interaction terms between all scatterers, and the second term on the right-hand side is vector $\mathbf{\Psi}$ containing the total wavefields arriving at each scatterer. In compact form, this equation thus becomes

$$\mathbf{\Psi_0} = -\mathbf{M}\mathbf{\Psi} \ , \tag{2.5}$$

and since both $\mathbf{\Psi_0}$ and $\mathbf{M}$ can be calculated using equation (2.2) and the Green's function formulae in Appendix A.1, equation (2.5) can be solved numerically by matrix inversion:

$$\mathbf{\Psi} = -\mathbf{M}^{-1}\mathbf{\Psi_0} \ . \tag{2.6}$$

Equation (2.6) gives a vector containing the total field that reaches each scatterer. When inserted into equation (2.1), this term can therefore be used to evaluate the total field that reaches the receiver at $\mathbf{x}_R$.

The equations above thus provide an exact representation of the monopole wavefield through a scattering medium of constant background velocity produced by an impulsive source at $\mathbf{x}_S$ and recorded by a receiver at $\mathbf{x}_R$, including all orders of interactions between the scatterers. The only possible sources of inaccuracy in practice are numerical, due to the finite word storage length of a real number, and any approximation in the matrix inversion in equation (2.6). The inverse problem in equation (2.6) is solved in Matlab using the `mldivide` operation, which seeks a solution by performing a general triangular factorisation that uses LU decomposition of $\mathbf{M}$ with partial pivoting (MathWorks, 2012). If matrix $\mathbf{M}$ is singular, the solution to equation (2.6) either does not exist or it is non-unique. In all of our experiments, the inverse problem in equation (2.6) was always well-posed[2]. In the case of dipole (derivative) sources and receivers, as used for example in seismic interferometry (Wapenaar, 2004; van Manen et al., 2005, 2006; Wapenaar & Fokkema, 2006), equations

[2]If the solution to equation (2.6) is non-unique, a least-squares solution may be found by replacing the `mldivide` operation by `pinv` at lines 581-582 and 585-586 of `model_gfs_p_scat_acoust.m`.

(2.1)-(2.3) need to be slightly modified to take into account whether differentiation is performed at the source (to obtain a dipole source) or at the receiver (to obtain a dipole receiver). When dipole sources or receivers are used, the direct wavefield in equation (2.2) becomes

$$\begin{aligned}\Psi_0'(\mathbf{x}_R) &= \partial_m \Psi_0(\mathbf{x}_R) \\ &= s(\omega)\partial_m G(\mathbf{x}_R, \mathbf{x}_S) \ ,\end{aligned} \tag{2.7}$$

where $\partial_m G(\mathbf{x}_R, \mathbf{x}_S)$ is the partial derivative of the Green's function between source $\mathbf{x}_S$ and receiver $\mathbf{x}_R$ along the m-direction, evaluated at $\mathbf{x}_S$ for a dipole source and at $\mathbf{x}_R$ for a dipole receiver.

When differentiation is performed with respect to sources, from equation (2.3) we get

$$\Psi'(\mathbf{x}^{(i)}) = \Psi_0'(\mathbf{x}^{(i)}) + \sum_{\substack{j=1 \\ j\neq i}}^{N} \Psi'(\mathbf{x}^{(j)}) A^{(j)} G(\mathbf{x}^{(i)}, \mathbf{x}^{(j)}) \ , \tag{2.8}$$

where $\Psi_0'(\mathbf{x}^{(i)})$ is the direct dipole-source wavefield to scatterer (i). The total dipole-source wavefield recorded by receiver $\mathbf{x}_R$ is given by

$$\Psi'(\mathbf{x}_R) = \Psi_0'(\mathbf{x}_R) + \sum_{i=1}^{N} \Psi'(\mathbf{x}^{(i)}) A^{(i)} G(\mathbf{x}_R, \mathbf{x}^{(i)}) \ . \tag{2.9}$$

When differentiation is performed with respect to receivers, the total wavefield recorded by a dipole receiver at $\mathbf{x}_R$ is simply given by:

$$\Psi'(\mathbf{x}_R) = \Psi_0'(\mathbf{x}_R) + \sum_{i=1}^{N} \Psi(\mathbf{x}^{(i)}) A^{(i)} \partial_m G(\mathbf{x}_R, \mathbf{x}^{(i)}) \ , \tag{2.10}$$

where $\partial_m G(\mathbf{x}_R, \mathbf{x}^{(i)})$ is the partial derivative of the Green's function between scatterer (i) and receiver $\mathbf{x}_R$ evaluated along the m-direction at $\mathbf{x}_R$. Equations (2.7)-(2.10) can therefore be used to solve a similar inverse problem to that in equation (2.6), to obtain the total wavefield from source $\mathbf{x}_S$ to receiver $\mathbf{x}_R$ when dipole or derivative Green's functions are used.

2.2 Acoustic Green's Functions from Seismic Interferometry

The term *seismic interferometry* refers to a set of methods of constructing Green's functions by cross-correlation (Wapenaar, 2004; van Manen et al., 2005, 2006; Wapenaar & Fokkema, 2006), convolution (Slob et al., 2007; Slob & Wapenaar, 2007) or deconvolution (Vasconcelos & Snieder, 2008a,b; Wapenaar et al., 2008; Wapenaar & van der Neut, 2010; Wapenaar et al., 2011; Minato et al., 2011) of seismic wavefields. Inter-receiver interferometry by cross-correlation uses a boundary of seismic sources (active sources such as dynamite or

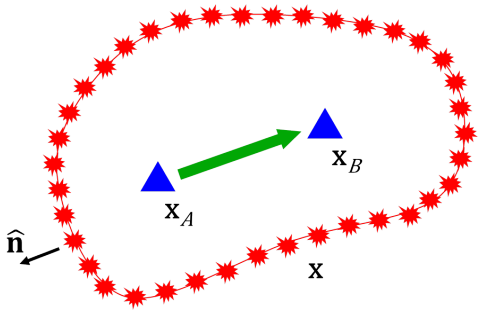

Figure 2.2. Schematic illustration of a typical geometry for correlational seismic interferometry. Two receivers (blue triangles) are surrounded by a boundary of sources (red explosions); at each source position, the boundary normal is denoted by $\hat{\mathbf{n}}$. The method of seismic interferometry uses one of the receivers (e.g. $\mathbf{x}_A$) as a 'virtual' (imagined) source, and constructs the signal (Green's function) as though this source was recorded by the other receiver (e.g. $\mathbf{x}_B$).

passive sources such as microseisms), to construct the Green's function between pairs of receivers located within the boundary as though one of the receivers had actually been a source that was recorded by the other receiver (figure 2.2).

Interferometry is a good field of application to test and demonstrate the Foldy code as it is a field in rapid development where new algorithms are being developed monthly (for reviews see Curtis et al. (2006), Wapenaar et al. (2010a,b), Galetti & Curtis (2012)). Since it is exact, the Foldy method of acoustic wavefield modelling is useful for testing these new algorithms. This is particularly true because, as we shall see, improvements and deficiencies associated with each algorithm may only be subtly different from those of other algorithms, implying that the accuracy of the modelling code used for testing is paramount.

Acoustic interferometric modelling formulae in the inter-receiver case have so far been derived by Wapenaar & Fokkema (2006) and van Manen et al. (2005). However, due to differences in the type of sources used in the two studies and to a different sign convention in the source term, the interferometric equations resulting from the two papers differ slightly. In this section, the differences between the two approaches are described and the resulting interferometric modelling formulae are given in both the frequency and time domain.

In all subsequent formulae, the following symbols and conventions are used: ρ and c are the medium density and propagation velocity; $\iota = \sqrt{-1}$ is the imaginary unit; the superscript star * denotes complex conjugation in the frequency domain (equivalent to time-reversal in the time domain, if applied to all terms in the FT of a time series); $\otimes$ denotes convolution (which is equivalent to crosscorrelation when one of the two signals is time-reversed); ∂_j represents partial differentiation in the x_j-direction with respect to the source coordinate; n_j is the component of the boundary normal along the x_j-direction; G and $\partial_j G$ represent Green's functions as responses to monopole and dipole sources; $\iota\omega$ and $\frac{1}{\iota\omega}$ denote differentiation and integration over time performed in the frequency domain, respectively.

2.2.1 Interferometric Formulae for Volume Injection Sources

Interferometric modelling formulae for volume injection sources are derived by Wapenaar & Fokkema (2006) and van Manen et al. (2005). The sign difference between equations (21) and (32) in Wapenaar & Fokkema (2006) and equation (4) in van Manen et al. (2005)) is given by a difference in sign in the source term used in the two papers.

Wapenaar & Fokkema (2006)

Wapenaar & Fokkema (2006) choose impulsive point sources of volume injection (denoted by a hat symbol$\hat{}$) which are defined as:

$$\hat{q}_0 = \frac{\delta(\mathbf{x} - \mathbf{x}_0)}{\iota\omega} \,, \tag{2.11}$$

where the subscript $_0$ can be used to denote either A or B. From the acoustic reciprocity theorem of the correlation type they obtain the following expressions representing the difference between the Green's function from $\mathbf{x}_A$ to $\mathbf{x}_B$ and its complex conjugate (or time-reverse in the time domain):

$$\begin{aligned}&\hat{G}(\mathbf{x}_B, \mathbf{x}_A, \omega) - \hat{G}^*(\mathbf{x}_B, \mathbf{x}_A, \omega) \\ &= \int_S \frac{1}{\rho(\mathbf{x})} \left[\left(\partial_j \hat{G}(\mathbf{x}_B, \mathbf{x}, \omega) \right) \hat{G}^*(\mathbf{x}_A, \mathbf{x}, \omega) - \hat{G}(\mathbf{x}_B, \mathbf{x}, \omega) \left(\partial_j \hat{G}^*(\mathbf{x}_A, \mathbf{x}, \omega) \right) \right] n_j \, \mathrm{d}S\end{aligned} \tag{2.12}$$

in the frequency domain, and

$$\begin{aligned}&\hat{G}(\mathbf{x}_B, \mathbf{x}_A, t) - \hat{G}(\mathbf{x}_B, \mathbf{x}_A, -t) \\ &= \int_S \frac{1}{\rho(\mathbf{x})} \left[\left(\partial_j \hat{G}(\mathbf{x}_B, \mathbf{x}, t) \right) \otimes \hat{G}(\mathbf{x}_A, \mathbf{x}, -t) - \hat{G}(\mathbf{x}_B, \mathbf{x}, t) \otimes \left(\partial_j \hat{G}(\mathbf{x}_A, \mathbf{x}, -t) \right) \right] n_j \, \mathrm{d}S\end{aligned} \tag{2.13}$$

in the time domain. By assuming a high frequency regime, that the bounding surface S is a sphere with very large radius, and that no energy scatters back through the boundary once it has left, equations (2.12) and (2.13) can be simplified using the Sommerfield radiation conditions to eliminate the derivatives, giving:

$$\hat{G}(\mathbf{x}_B, \mathbf{x}_A, \omega) - \hat{G}^*(\mathbf{x}_B, \mathbf{x}_A, \omega) \approx -\frac{2\iota\omega}{\rho c} \int_S \hat{G}(\mathbf{x}_B, \mathbf{x}, \omega) \hat{G}^*(\mathbf{x}_A, \mathbf{x}, \omega) \, \mathrm{d}S \tag{2.14}$$

in the frequency domain, and

$$\hat{G}(\mathbf{x}_B, \mathbf{x}_A, t) - \hat{G}(\mathbf{x}_B, \mathbf{x}_A, -t) \approx -\frac{2}{\rho c}\frac{\mathrm{d}}{\mathrm{d}t}\left\{\int_S \hat{G}(\mathbf{x}_B, \mathbf{x}, t) \otimes \hat{G}(\mathbf{x}_A, \mathbf{x}, -t)\,\mathrm{d}S\right\} \quad (2.15)$$

in the time domain.

van Manen et al. (2005)

van Manen et al. (2005) choose impulsive point sources of volume injection (denoted by an upside-down hat symbol $\check{}$) which are defined as:

$$\check{q}_0 = -\frac{\delta(\mathbf{x} - \mathbf{x}_0)}{\iota\omega}\,, \quad (2.16)$$

where the subscript $_0$ can be used to denote either A or B. From the acoustic reciprocity theorem of the correlation type they obtain the following expressions representing the difference between the complex conjugate of the Green's function between $\mathbf{x}_A$ and $\mathbf{x}_B$ and the Green's function between $\mathbf{x}_A$ and $\mathbf{x}_B$:

$$\begin{aligned}&\check{G}^*(\mathbf{x}_B, \mathbf{x}_A, \omega) - \check{G}(\mathbf{x}_B, \mathbf{x}_A, \omega)\\ &= \int_S \frac{1}{\rho(\mathbf{x})}\left[\left(\partial_j \check{G}(\mathbf{x}_B, \mathbf{x}, \omega)\right)\check{G}^*(\mathbf{x}_A, \mathbf{x}, \omega) - \check{G}(\mathbf{x}_B, \mathbf{x}, \omega)\left(\partial_j \check{G}^*(\mathbf{x}_A, \mathbf{x}, \omega)\right)\right] n_j\,\mathrm{d}S\end{aligned} \quad (2.17)$$

in the frequency domain, and

$$\begin{aligned}&\check{G}(\mathbf{x}_B, \mathbf{x}_A, -t) - \check{G}(\mathbf{x}_B, \mathbf{x}_A, t)\\ &= \int_S \frac{1}{\rho(\mathbf{x})}\left[\left(\partial_j \check{G}(\mathbf{x}_B, \mathbf{x}, t)\right) \otimes \check{G}(\mathbf{x}_A, \mathbf{x}, -t) - \check{G}(\mathbf{x}_B, \mathbf{x}, t) \otimes \left(\partial_j \check{G}(\mathbf{x}_A, \mathbf{x}, -t)\right)\right] n_j\,\mathrm{d}S\end{aligned} \quad (2.18)$$

in the time domain. By assuming the same far-field conditions as for the Wapenaar & Fokkema (2006) equations above, equations (2.17) and (2.18) can be simplified to

$$\check{G}^*(\mathbf{x}_B, \mathbf{x}_A, \omega) - \check{G}(\mathbf{x}_B, \mathbf{x}_A, \omega) \approx -\frac{2\iota\omega}{\rho c}\int_S \check{G}(\mathbf{x}_B, \mathbf{x}, \omega)\check{G}^*(\mathbf{x}_A, \mathbf{x}, \omega)\,\mathrm{d}S \quad (2.19)$$

in the frequency domain, and

$$\check{G}(\mathbf{x}_B, \mathbf{x}_A, -t) - \check{G}(\mathbf{x}_B, \mathbf{x}_A, t) \approx -\frac{2}{\rho c}\frac{\mathrm{d}}{\mathrm{d}t}\left\{\int_S \check{G}(\mathbf{x}_B, \mathbf{x}, t) \otimes \check{G}(\mathbf{x}_A, \mathbf{x}, -t)\,\mathrm{d}S\right\} \quad (2.20)$$

in the time domain.

2.2.2 Interferometric Formulae for Volume Injection Rate Sources

Interferometric modelling formulae for volume injection rate sources are derived by Wapenaar & Fokkema (2006) but not by van Manen et al. (2005). However, they can easily be derived using the van Manen et al. (2005) approach and are therefore given in this section. Again, the sign difference in the solution arises from the different sign used in the source term.

Wapenaar & Fokkema (2006)

Wapenaar & Fokkema (2006) choose impulsive point sources of volume injection rate (denoted by a double hat symbol $\hat{\ }$) which are defined as:

$$\hat{\hat{q}}_0 = \delta(\mathbf{x} - \mathbf{x}_0) \, , \tag{2.21}$$

where the subscript $_0$ can be used to denote either A or B. From the acoustic reciprocity theorem of the correlation type they obtain the following expressions representing the sum of the Green's function between $\mathbf{x}_A$ and $\mathbf{x}_B$ and its complex conjugate (or time-reverse in the time domain):

$$\begin{aligned}
&\hat{\hat{G}}(\mathbf{x}_B, \mathbf{x}_A, \omega) + \hat{\hat{G}}^*(\mathbf{x}_B, \mathbf{x}_A, \omega) \\
&= -\frac{1}{\iota\omega} \int\limits_S \frac{1}{\rho(\mathbf{x})} \left[\left(\partial_j \hat{\hat{G}}(\mathbf{x}_B, \mathbf{x}, \omega) \right) \hat{\hat{G}}^*(\mathbf{x}_A, \mathbf{x}, \omega) - \hat{\hat{G}}(\mathbf{x}_B, \mathbf{x}, \omega) \left(\partial_j \hat{\hat{G}}^*(\mathbf{x}_A, \mathbf{x}, \omega) \right) \right] n_j \, \mathrm{d}S
\end{aligned} \tag{2.22}$$

in the frequency domain, and

$$\begin{aligned}
&\hat{\hat{G}}(\mathbf{x}_B, \mathbf{x}_A, t) + \hat{\hat{G}}(\mathbf{x}_B, \mathbf{x}_A, -t) \\
&= -\int \left\{ \int\limits_S \frac{1}{\rho(\mathbf{x})} \left[\left(\partial_j \hat{\hat{G}}(\mathbf{x}_B, \mathbf{x}, t) \right) \otimes \hat{\hat{G}}(\mathbf{x}_A, \mathbf{x}, -t) - \hat{\hat{G}}(\mathbf{x}_B, \mathbf{x}, t) \otimes \left(\partial_j \hat{\hat{G}}(\mathbf{x}_A, \mathbf{x}, -t) \right) \right] n_j \, \mathrm{d}S \right\} \mathrm{d}t
\end{aligned} \tag{2.23}$$

in the time domain. By assuming the same conditions as in section 2.2.1, equations (2.22) and (2.23) can be simplified to

$$\hat{\hat{G}}(\mathbf{x}_B, \mathbf{x}_A, \omega) + \hat{\hat{G}}^*(\mathbf{x}_B, \mathbf{x}_A, \omega) \approx \frac{2}{\rho c} \int\limits_S \hat{\hat{G}}(\mathbf{x}_B, \mathbf{x}, \omega) \hat{\hat{G}}^*(\mathbf{x}_A, \mathbf{x}, \omega) \, \mathrm{d}S \tag{2.24}$$

in the frequency domain, and

$$\hat{\hat{G}}(\mathbf{x}_B, \mathbf{x}_A, t) + \hat{\hat{G}}(\mathbf{x}_B, \mathbf{x}_A, -t) \approx \frac{2}{\rho c} \int\limits_S \hat{\hat{G}}(\mathbf{x}_B, \mathbf{x}, t) \otimes \hat{\hat{G}}(\mathbf{x}_A, \mathbf{x}, -t) \, \mathrm{d}S \tag{2.25}$$

in the time domain.

A van Manen et al. (2005)-like approach

Similarly to the previous case, impulsive point sources of volume injection rate (denoted by an upside-down double hat symbol $\breve{}$) can be defined as:

$$\breve{\breve{q}}_0 = -\delta(\mathbf{x} - \mathbf{x}_0) \ , \tag{2.26}$$

where the subscript $_0$ can be used to denote either A or B. From the acoustic reciprocity theorem of the correlation type, the following expressions representing the sum of the Green's function between $\mathbf{x}_A$ and $\mathbf{x}_B$ and its complex conjugate (or time-reverse in the time domain) can be obtained:

$$\begin{aligned}&\breve{\breve{G}}(\mathbf{x}_B, \mathbf{x}_A, \omega) + \breve{\breve{G}}^*(\mathbf{x}_B, \mathbf{x}_A, \omega) \\ &= \frac{1}{\iota\omega} \int\limits_S \frac{1}{\rho(\mathbf{x})} \left[\left(\partial_j \breve{\breve{G}}(\mathbf{x}_B, \mathbf{x}, \omega) \right) \breve{\breve{G}}^*(\mathbf{x}_A, \mathbf{x}, \omega) - \breve{\breve{G}}(\mathbf{x}_B, \mathbf{x}, \omega) \left(\partial_j \breve{\breve{G}}^*(\mathbf{x}_A, \mathbf{x}, \omega) \right) \right] n_j \, \mathrm{d}S\end{aligned} \tag{2.27}$$

in the frequency domain, and

$$\begin{aligned}&\breve{\breve{G}}(\mathbf{x}_B, \mathbf{x}_A, t) + \breve{\breve{G}}(\mathbf{x}_B, \mathbf{x}_A, -t) \\ &= \int \left\{ \int\limits_S \frac{1}{\rho(\mathbf{x})} \left[\left(\partial_j \breve{\breve{G}}(\mathbf{x}_B, \mathbf{x}, t) \right) \otimes \breve{\breve{G}}(\mathbf{x}_A, \mathbf{x}, -t) - \breve{\breve{G}}(\mathbf{x}_B, \mathbf{x}, t) \otimes \left(\partial_j \breve{\breve{G}}(\mathbf{x}_A, \mathbf{x}, -t) \right) \right] n_j \, \mathrm{d}S \right\} \mathrm{d}t\end{aligned} \tag{2.28}$$

in the time domain. By assuming the same conditions as in section 2.2.1, equations (2.27) and (2.28) can be simplified to

$$\breve{\breve{G}}(\mathbf{x}_B, \mathbf{x}_A, \omega) + \breve{\breve{G}}^*(\mathbf{x}_B, \mathbf{x}_A, \omega) \approx -\frac{2}{\rho c} \int\limits_S \breve{\breve{G}}(\mathbf{x}_B, \mathbf{x}, \omega) \breve{\breve{G}}^*(\mathbf{x}_A, \mathbf{x}, \omega) \, \mathrm{d}S \tag{2.29}$$

in the frequency domain, and

$$\breve{\breve{G}}(\mathbf{x}_B, \mathbf{x}_A, t) + \breve{\breve{G}}(\mathbf{x}_B, \mathbf{x}_A, -t) \approx -\frac{2}{\rho c} \int\limits_S \breve{\breve{G}}(\mathbf{x}_B, \mathbf{x}, t) \otimes \breve{\breve{G}}(\mathbf{x}_A, \mathbf{x}, -t) \, \mathrm{d}S \tag{2.30}$$

in the time domain.

2.2.3 Other Types of Interferometry

The interferometric formulae in the previous section can be used for the method of *inter-receiver interferometry*, i.e. a Green's function retrieval method that uses boundaries of sources to construct the Green's function between pairs of enclosed receivers. By applying source-receiver reciprocity, the position of sources and receivers can be exchanged: this leads to the derivation of interferometric formulae that can be used for *inter-source interferometry*, which uses a boundary of receivers to construct the Green's function between pairs of enclosed sources, and *source-receiver interferometry*, which uses boundaries of sources and receivers to construct the Green's function between an enclosed source and receiver. Interferometric formulae for inter-source and source-receiver interferometry, together with examples of wavefield modelling and its application to inter-source and source-receiver interferometry, are given in sections 2.4 and 2.5.

2.3 Worked Examples

The modelling code package contains five examples showing how inter-receiver, inter-source and source-receiver interferometry can be applied to the modelling results: in examples 1-3, the Green's function between a virtual source and a receiver (examples 1 and 2) or an array of receivers (example 3) is calculated using interferometry from a circular boundary of surrounding sources; in example 4, the Green's function between a source and a virtual receiver is calculated using interferometry from a circular boundary of surrounding receivers; in example 5, the Green's function between a source and a receiver is calculated using interferometry from two circular boundaries of surrounding sources and receivers. As shown by the interferometric formulae in section 2.2, interferometry can be performed in both the frequency domain (multiplication) and in the time domain (crosscorrelation). While example 1 uses time-domain crosscorrelation, examples 2-5 use frequency-domain crosscorrelation, since the latter is generally more computationally efficient.

2.3.1 Example 1 - Inter-Receiver Interferometry in Time Domain

Run by executing the Matlab script `example_1__inter_receiver_T.m`. With the given settings, the figures shown in Fig. 2.3, Fig. 2.4 and Fig. 2.5 are obtained. In this case, a negative volume injection source is used, and interferometry is performed in the time-domain using the van Manen et al. (2005) formula in equation (2.18). As indicated by the formula, the causal (positive-time) part of the interferometric Green's function is the negative of the exact result modelled by placing a source at A and a receiver at B, while the acausal (negative-time) part of the interferometric Green's function matches the time-reverse of the true modelled result.

Note: when interferometry is performed using the formulae in equations (2.15), (2.20), (2.23), (2.28) (i.e. by changing `method` and `inttype`), differentiation/integration over time

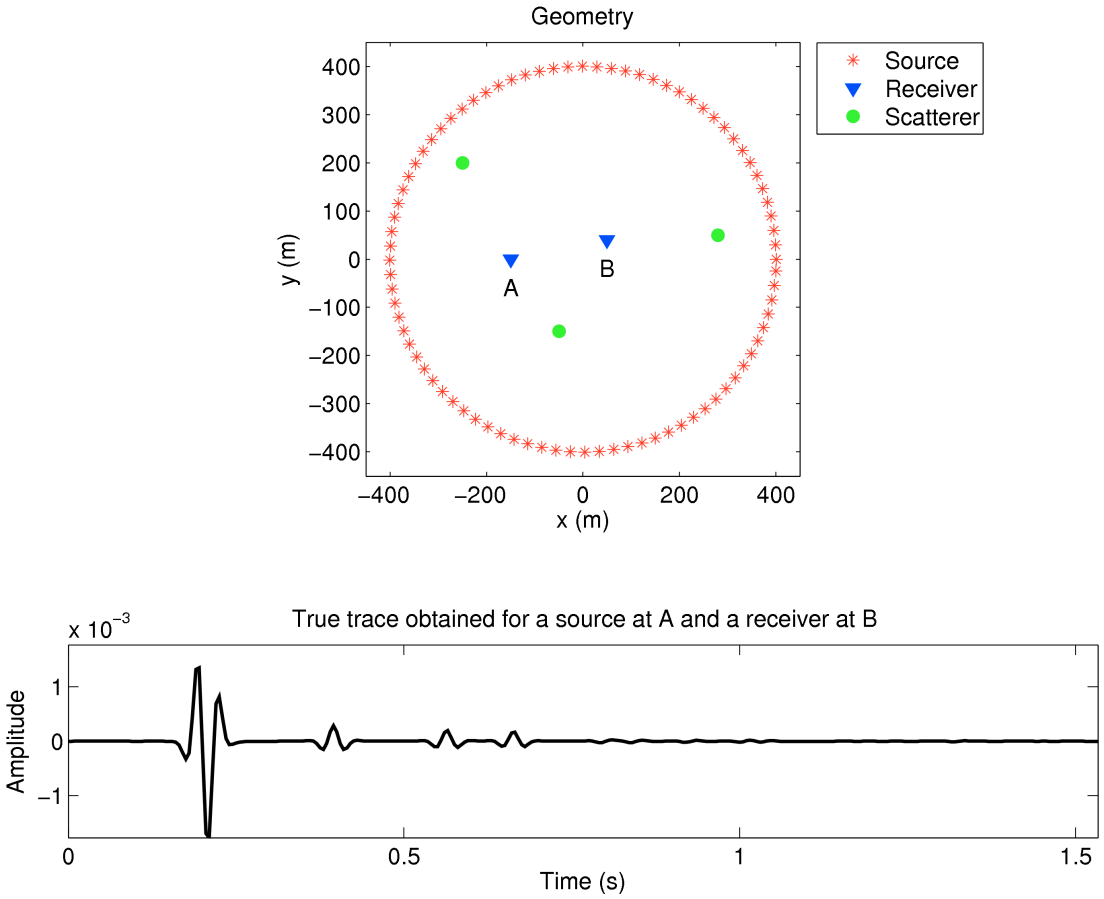

Figure 2.3. Geometry and true modelled trace in examples 1 and 2. Only every sixth source is plotted for clarity.

has to be performed in the time domain using the Matlab functions `cumtrapz` and `gradient`. This introduces errors in the reconstructed Green's function which are not present if interferometry is performed in the frequency domain (where differentiation and integration are performed by multiplication and division by $\iota\omega$, respectively).

2.3.2 Example 2 - Inter-Receiver Interferometry in Frequency Domain

Run by executing the Matlab script `example_2_inter_receiver_F.m`. With the given settings, the figures shown in Fig. 2.3, Fig. 2.4 and Fig. 2.5 are obtained (same figures as the previous example, as the two examples produce identical results). In this case, a negative volume injection source is used, and interferometry is performed in the frequency-domain using the van Manen et al. (2005) formula in equation (2.17). As indicated by the formula, the causal (positive-time) part of the interferometric Green's function is the negative of the exact result modelled by placing a source at A and a receiver at B, while the acausal (negative-time) part of the interferometric Green's function matches the time-reverse of the true modelled result.

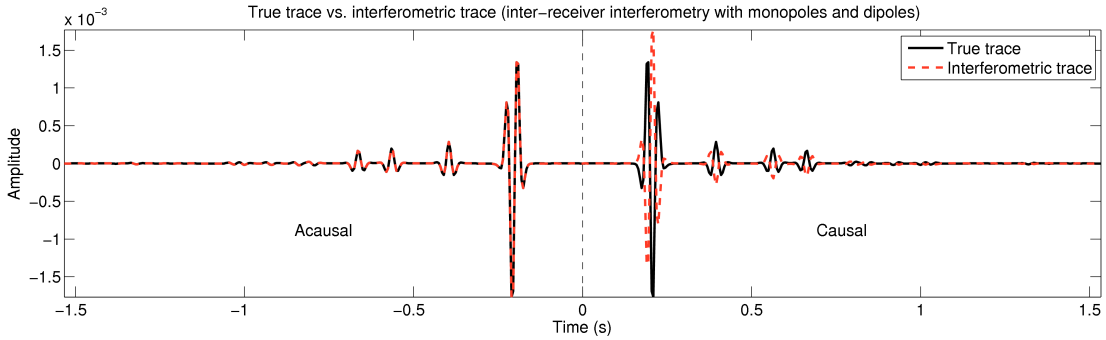

Figure 2.4. True trace and interferometric trace in both examples 1 and 2 (results are identical in the two examples). When interferometry is performed using the van Manen et al. (2005) formulae in equations (2.17) and (2.18), the causal part of the interferometric trace matches the negative of the true trace, while the acausal part of the interferometric trace matches the time-reverse of the true trace.

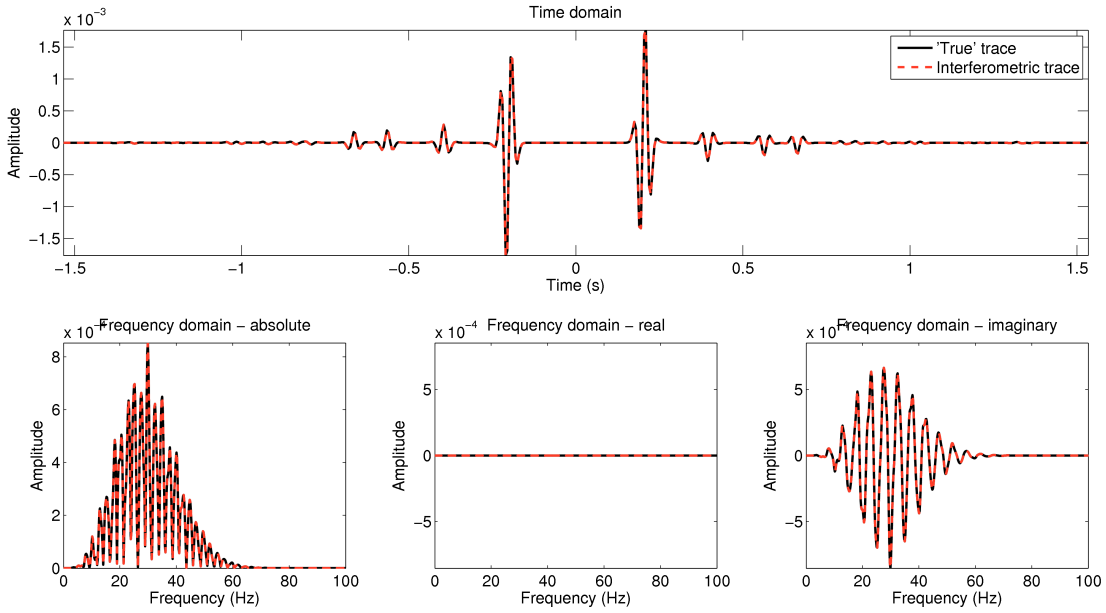

Figure 2.5. 'True' trace and interferometric trace in examples 1 and 2 as above. Top: the causal part of the 'true' trace is obtained by taking the negative of the true trace in Fig. 2.3, while the acausal part is obtained by time-reversing the true trace in Fig. 2.3, according to the van Manen et al. (2005) formulae in equations (2.17) and (2.18). Bottom left: frequency spectra. Bottom centre: real component of frequency - equal to zero when using the interferometric formulae in equations (2.17) and (2.18). Bottom right: imaginary component of frequency.

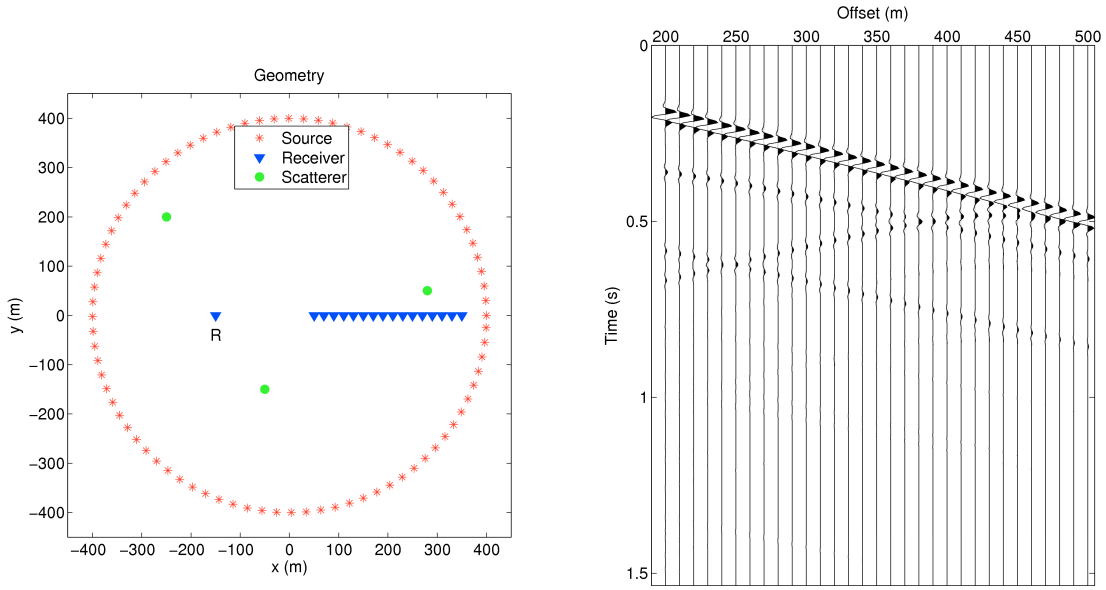

Figure 2.6. Geometry and true traces modelled between a source positioned at the location of receiver R and the receiver array shown (example 3). In the left panel, only every sixth source and every second receiver are plotted for clarity.

2.3.3 Example 3 - Inter-Receiver Interferometry with an Array of Receivers

Run by executing the Matlab script `example_3__inter_receiver_F_array.m`. With the given settings, the figures shown in Fig. 2.6 and Fig. 2.7 are obtained. In this case, a negative volume injection source is used, and interferometry is performed in the frequency-domain using the van Manen et al. (2005) formula in equation (2.17). The wiggle plot is obtained using function `wiggles.m`, which is included in the package as part of this example. As indicated by the formula, the causal (positive-time) parts of the interferometric Green's functions are the negative of the exact results modelled by placing a source at R and recording the signals at the receiver array, while the acausal (negative-time) parts of the interferometric Green's functions match the time-reverse of the true modelled results. Fig. 2.7 also shows the direct comparison of signals recorded and reconstructed at the array receiver located 280 m from R.

2.4 Inter-Source Interferometry

The method of inter-source interferometry uses a boundary of receivers to construct the Green's function between pairs of enclosed sources (Fig. 2.8, top panel). For this configuration, interferometric formulae can be obtained directly from inter-receiver interferometry formulae by exchanging the position of sources (in this case $\mathbf{x}_A$ and $\mathbf{x}_B$) and receivers (in this case located on boundary S and denoted by $\mathbf{x}$). A detailed description of the method of inter-source interferometry is given by Curtis et al. (2009).

Inter-source interferometric formulae for volume injection and volume injection rate sources, obtained using the van Manen et al. (2005) and Wapenaar & Fokkema (2006) approaches, are

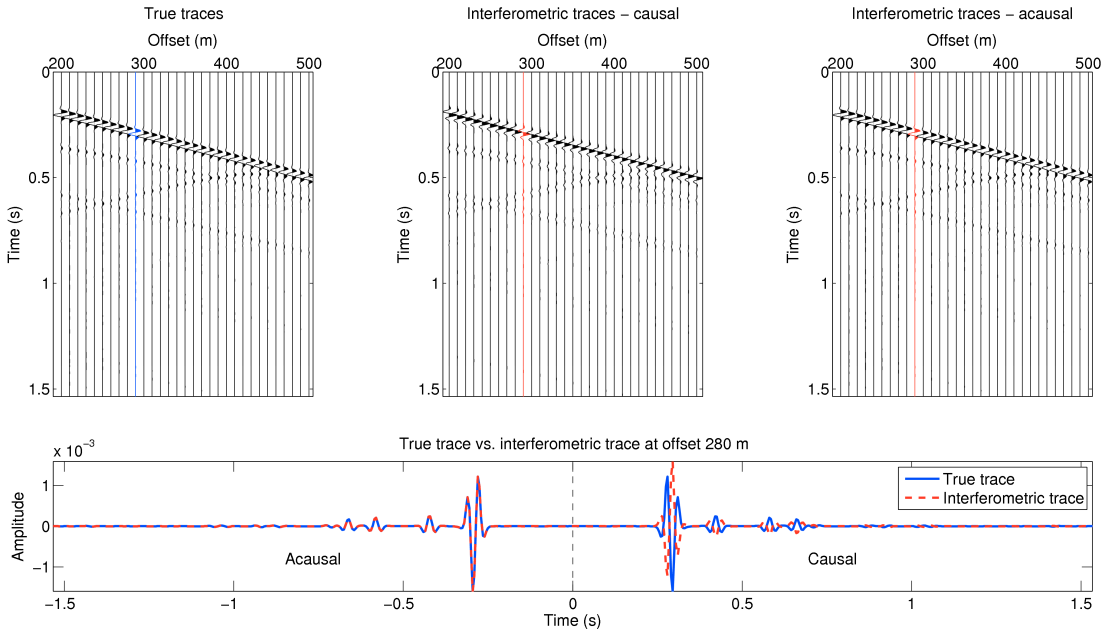

Figure 2.7. True traces and interferometric traces in example 3. Top: the causal part of the interferometric traces matches the negative of the true traces, while the time-reverse of the acausal part of the interferometric traces matches the true traces, according to equation (2.17). Bottom: comparison of true and interferometric trace for a receiver at 280 m offset.

listed below (in the frequency domain only). Note that, contrary to the inter-receiver formulae above, in this case the derivatives ∂_j are taken at the receiver side:

- Volume injection sources, Wapenaar & Fokkema (2006) approach, monopole and dipole receivers:

$$\begin{aligned}&\hat{G}(\mathbf{x}_B,\mathbf{x}_A,\omega)-\hat{G}^*(\mathbf{x}_B,\mathbf{x}_A,\omega)\\&=\int_S\frac{1}{\rho(\mathbf{x})}\left[\left(\partial_j\hat{G}(\mathbf{x},\mathbf{x}_B,\omega)\right)\hat{G}^*(\mathbf{x},\mathbf{x}_A,\omega)-\hat{G}(\mathbf{x},\mathbf{x}_B,\omega)\left(\partial_j\hat{G}^*(\mathbf{x},\mathbf{x}_A,\omega)\right)\right]n_j\,\mathrm{d}S\end{aligned} \tag{2.31}$$

- Volume injection sources, Wapenaar & Fokkema (2006) approach, monopole receivers only:

$$\hat{G}(\mathbf{x}_B,\mathbf{x}_A,\omega)-\hat{G}^*(\mathbf{x}_B,\mathbf{x}_A,\omega)\approx-\frac{2\imath\omega}{\rho c}\int_S\hat{G}(\mathbf{x},\mathbf{x}_B,\omega)\hat{G}^*(\mathbf{x},\mathbf{x}_A,\omega)\,\mathrm{d}S \tag{2.32}$$

- Volume injection sources, van Manen et al. (2005) approach, monopole and dipole receivers

(Curtis et al., 2009):

$$\begin{aligned}&\check{G}^{*}(\mathbf{x}_B,\mathbf{x}_A,\omega)-\check{G}(\mathbf{x}_B,\mathbf{x}_A,\omega)\\&=\int\limits_S\frac{1}{\rho(\mathbf{x})}\left[\left(\partial_j\check{G}(\mathbf{x},\mathbf{x}_B,\omega)\right)\check{G}^{*}(\mathbf{x},\mathbf{x}_A,\omega)-\check{G}(\mathbf{x},\mathbf{x}_B,\omega)\left(\partial_j\check{G}^{*}(\mathbf{x},\mathbf{x}_A,\omega)\right)\right]n_j\,\mathrm{d}S\end{aligned} \tag{2.33}$$

- Volume injection sources, van Manen et al. (2005) approach, monopole receivers only (Curtis et al., 2009):

$$\check{G}^{*}(\mathbf{x}_B,\mathbf{x}_A,\omega)-\check{G}(\mathbf{x}_B,\mathbf{x}_A,\omega)\approx-\frac{2\iota\omega}{\rho c}\int\limits_S\check{G}(\mathbf{x},\mathbf{x}_B,\omega)\check{G}^{*}(\mathbf{x},\mathbf{x}_A,\omega)\,\mathrm{d}S \tag{2.34}$$

- Volume injection rate sources, Wapenaar & Fokkema (2006) approach, monopole and dipole receivers:

$$\begin{aligned}&\hat{\check{G}}(\mathbf{x}_B,\mathbf{x}_A,\omega)+\hat{\check{G}}^{*}(\mathbf{x}_B,\mathbf{x}_A,\omega)\\&=-\frac{1}{\iota\omega}\int\limits_S\frac{1}{\rho(\mathbf{x})}\left[\left(\partial_j\hat{\check{G}}(\mathbf{x},\mathbf{x}_B,\omega)\right)\hat{\check{G}}^{*}(\mathbf{x},\mathbf{x}_A,\omega)-\hat{\check{G}}(\mathbf{x},\mathbf{x}_B,\omega)\left(\partial_j\hat{\check{G}}^{*}(\mathbf{x},\mathbf{x}_A,\omega)\right)\right]n_j\,\mathrm{d}S\end{aligned} \tag{2.35}$$

- Volume injection rate sources, Wapenaar & Fokkema (2006) approach, monopole receivers only:

$$\hat{\check{G}}(\mathbf{x}_B,\mathbf{x}_A,\omega)+\hat{\check{G}}^{*}(\mathbf{x}_B,\mathbf{x}_A,\omega)\approx\frac{2}{\rho c}\int\limits_S\hat{\check{G}}(\mathbf{x},\mathbf{x}_B,\omega)\hat{\check{G}}^{*}(\mathbf{x},\mathbf{x}_A,\omega)\,\mathrm{d}S \tag{2.36}$$

- Volume injection rate sources, van Manen et al. (2005)-like approach, monopole and dipole receivers:

$$\begin{aligned}&\breve{\check{G}}(\mathbf{x}_B,\mathbf{x}_A,\omega)+\breve{\check{G}}^{*}(\mathbf{x}_B,\mathbf{x}_A,\omega)\\&=\frac{1}{\iota\omega}\int\limits_S\frac{1}{\rho(\mathbf{x})}\left[\left(\partial_j\breve{\check{G}}(\mathbf{x},\mathbf{x}_B,\omega)\right)\breve{\check{G}}^{*}(\mathbf{x},\mathbf{x}_A,\omega)-\breve{\check{G}}(\mathbf{x},\mathbf{x}_B,\omega)\left(\partial_j\breve{\check{G}}^{*}(\mathbf{x},\mathbf{x}_A,\omega)\right)\right]n_j\,\mathrm{d}S\end{aligned} \tag{2.37}$$

- Volume injection rate sources, van Manen et al. (2005)-like approach, monopole receivers only:

$$\breve{\check{G}}(\mathbf{x}_B,\mathbf{x}_A,\omega)+\breve{\check{G}}^{*}(\mathbf{x}_B,\mathbf{x}_A,\omega)\approx-\frac{2}{\rho c}\int\limits_S\breve{\check{G}}(\mathbf{x},\mathbf{x}_B,\omega)\breve{\check{G}}^{*}(\mathbf{x},\mathbf{x}_A,\omega)\,\mathrm{d}S \tag{2.38}$$

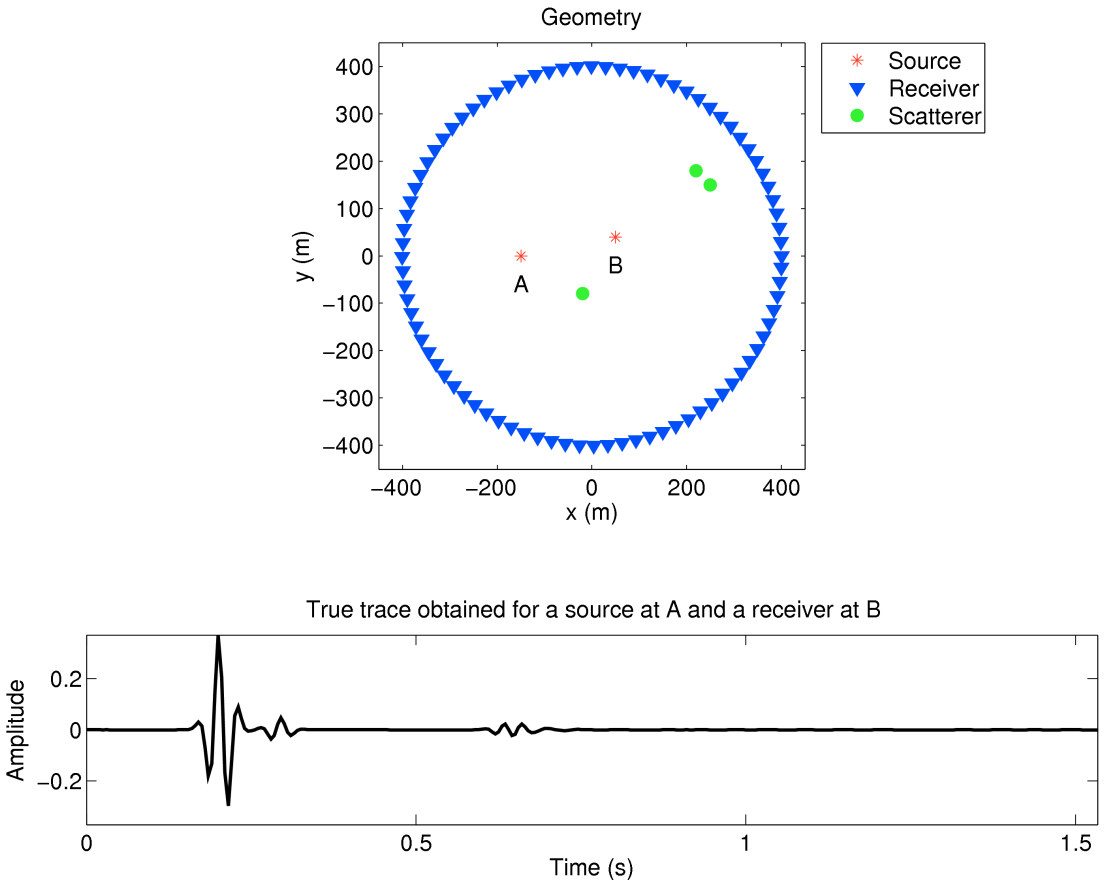

Figure 2.8. Geometry and true modelled trace in example 4. Only every sixth receiver is plotted for clarity.

2.4.1 Example 4 - Inter-Source Interferometry in Frequency Domain

Run by executing the Matlab script `example_4_inter_source_F.m`. With the given settings, the figures shown in Fig. 2.8, Fig. 2.9 and Fig. 2.10 are obtained. In this case, a positive volume injection rate source is used, and interferometry is performed in the frequency-domain using the formula in equation (2.35). As indicated by the formula, the causal (positive-time) part of the interferometric Green's function matches the exact result modelled by placing a source at A and a receiver at B, while the acausal (negative-time) part of the interferometric Green's function matches the time-reverse of the true modelled result.

2.5 Source-Receiver Interferometry

The method of source-receiver interferometry uses a boundary of sources and a boundary of receivers to construct the Green's function between an enclosed source and receiver (Fig. 2.11, top panel). For this configuration, interferometric formulae can be obtained by combining inter-receiver and inter-source interferometry equations and denoting the sources

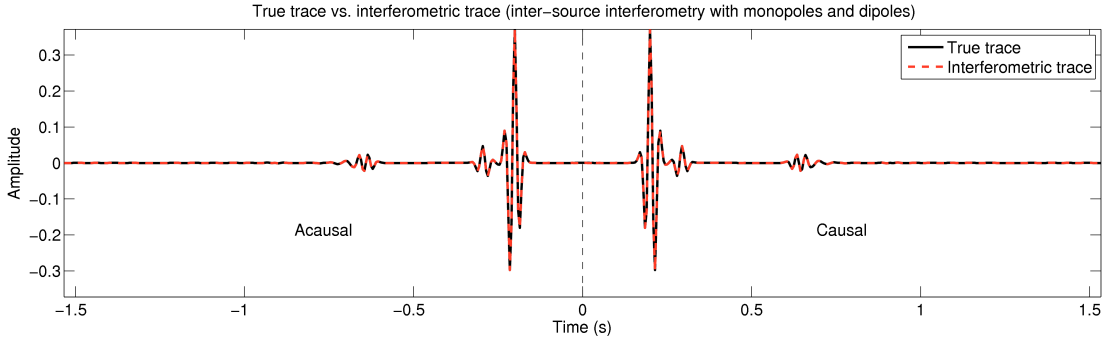

Figure 2.9. True trace and interferometric trace in example 4. When interferometry is performed using the formula in equation (2.35), the causal part of the interferometric trace matches the true trace, while the acausal part of the interferometric trace matches the time-reverse of the true trace.

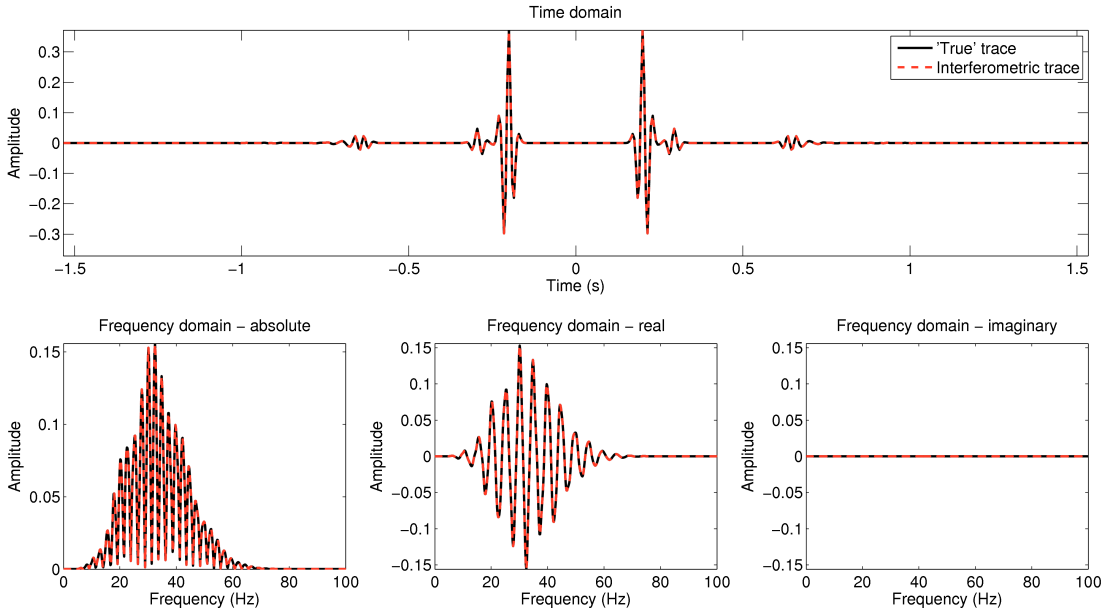

Figure 2.10. 'True' trace and interferometric trace in example 4. Top: the causal part of the 'true' trace is the modelled trace in Fig. 2.8, while the acausal part is obtained by time-reversing the true trace in Fig. 2.8, according to the formula in equation (2.35). Bottom left: frequency spectra. Bottom centre: real component of frequency. Bottom right: imaginary component of frequency - equal to zero when using the interferometric formula in equation (2.35).

on boundary S by $\mathbf{x}$, the receivers on boundary S' by $\mathbf{x}'$, and the central source and receiver by $\mathbf{x}_A$ and $\mathbf{x}_B$, respectively. A detailed description of the method of source-receiver interferometry is given by Curtis & Halliday (2010).
Source-receiver interferometric formulae for volume injection and volume injection rate sources, obtained using the van Manen et al. (2005) and Wapenaar & Fokkema (2006) approaches, are listed below (in the frequency domain only). Note that in this case the derivative ∂_j is taken with respect to the source boundary S, while the derivative $\partial_{j'}$ is taken with respect to the receiver boundary S':

- Volume injection sources, Wapenaar & Fokkema (2006) approach, monopole and dipole sources and receivers:

$$\begin{aligned}
&\hat{G}(\mathbf{x}_B,\mathbf{x}_A,\omega) - \hat{G}^*(\mathbf{x}_B,\mathbf{x}_A,\omega) \\
&\quad= \int_{S'} \frac{1}{\rho(\mathbf{x}')} \Bigg\{ \Bigg(\partial_{j'} \Bigg[\int_S \frac{1}{\rho(\mathbf{x})} \Big[\Big(\partial_j \hat{G}(\mathbf{x}',\mathbf{x},\omega) \Big) \hat{G}^*(\mathbf{x}_B,\mathbf{x},\omega) \\
&\quad -\hat{G}(\mathbf{x}',\mathbf{x},\omega) \Big(\partial_j \hat{G}^*(\mathbf{x}_B,\mathbf{x},\omega) \Big) \Big] n_j \,\mathrm{d}S \Bigg] \Bigg) \hat{G}^*(\mathbf{x}',\mathbf{x}_A,\omega) \\
&\quad - \Bigg[\int_S \frac{1}{\rho(\mathbf{x})} \Big[\Big(\partial_j \hat{G}(\mathbf{x}',\mathbf{x},\omega) \Big) \hat{G}^*(\mathbf{x}_B,\mathbf{x},\omega) \\
&\quad -\hat{G}(\mathbf{x}',\mathbf{x},\omega) \Big(\partial_j \hat{G}^*(\mathbf{x}_B,\mathbf{x},\omega) \Big) \Big] n_j \,\mathrm{d}S \Bigg] \Big(\partial_{j'} \hat{G}^*(\mathbf{x}',\mathbf{x}_A,\omega) \Big) \Bigg\} n_{j'} \,\mathrm{d}S'
\end{aligned} \tag{2.39}$$

- Volume injection sources, Wapenaar & Fokkema (2006) approach, monopole sources and receivers only:

$$\begin{aligned}
&\hat{G}(\mathbf{x}_B,\mathbf{x}_A,\omega) - \hat{G}^*(\mathbf{x}_B,\mathbf{x}_A,\omega) \\
&\quad\approx -\frac{2\iota\omega}{\rho c} \int_{S'} \Bigg[-\frac{2\iota\omega}{\rho c} \int_S \hat{G}(\mathbf{x}',\mathbf{x},\omega) \hat{G}^*(\mathbf{x}_B,\mathbf{x},\omega) \,\mathrm{d}S \Bigg] \hat{G}^*(\mathbf{x}',\mathbf{x}_A,\omega) \,\mathrm{d}S'
\end{aligned} \tag{2.40}$$

- Volume injection sources, van Manen et al. (2005) approach, monopole and dipole sources

and receivers (Curtis & Halliday, 2010):

$$\begin{aligned}
&\check{G}^{*}(\mathbf{x}_B,\mathbf{x}_A,\omega) - \check{G}(\mathbf{x}_B,\mathbf{x}_A,\omega) \\
&\quad= \int\limits_{S'} \frac{1}{\rho(\mathbf{x}')} \Bigg\{ \Bigg(\partial_{j'} \Bigg[\int\limits_{S} \frac{1}{\rho(\mathbf{x})} \left[\left(\partial_j \check{G}(\mathbf{x}',\mathbf{x},\omega)\right) \check{G}^{*}(\mathbf{x}_B,\mathbf{x},\omega) \right. \\
&\quad\quad \left. - \check{G}(\mathbf{x}',\mathbf{x},\omega) \left(\partial_j \check{G}^{*}(\mathbf{x}_B,\mathbf{x},\omega)\right) \right] n_j \,\mathrm{d}S \Bigg] \Bigg) \check{G}^{*}(\mathbf{x}',\mathbf{x}_A,\omega) \\
&\quad\quad - \Bigg[\int\limits_{S} \frac{1}{\rho(\mathbf{x})} \left[\left(\partial_j \check{G}(\mathbf{x}',\mathbf{x},\omega)\right) \check{G}^{*}(\mathbf{x}_B,\mathbf{x},\omega) \right. \\
&\quad\quad \left. - \check{G}(\mathbf{x}',\mathbf{x},\omega) \left(\partial_j \check{G}^{*}(\mathbf{x}_B,\mathbf{x},\omega)\right) \right] n_j \,\mathrm{d}S \Bigg] \left(\partial_{j'} \check{G}^{*}(\mathbf{x}',\mathbf{x}_A,\omega)\right) \Bigg\} n_{j'} \,\mathrm{d}S'
\end{aligned} \tag{2.41}$$

- Volume injection sources, van Manen et al. (2005) approach, monopole sources and receivers only (Curtis & Halliday, 2010):

$$\begin{aligned}
&\check{G}^{*}(\mathbf{x}_B,\mathbf{x}_A,\omega) - \check{G}(\mathbf{x}_B,\mathbf{x}_A,\omega) \\
&\quad\approx -\frac{2\iota\omega}{\rho c} \int\limits_{S'} \left[-\frac{2\iota\omega}{\rho c} \int\limits_{S} \check{G}(\mathbf{x}',\mathbf{x},\omega) \check{G}^{*}(\mathbf{x}_B,\mathbf{x},\omega) \,\mathrm{d}S \right] \check{G}^{*}(\mathbf{x}',\mathbf{x}_A,\omega) \,\mathrm{d}S'
\end{aligned} \tag{2.42}$$

- Volume injection rate sources, Wapenaar & Fokkema (2006) approach, monopole and dipole sources and receivers:

$$\begin{aligned}
&\hat{\check{G}}(\mathbf{x}_B,\mathbf{x}_A,\omega) + \hat{\check{G}}^{*}(\mathbf{x}_B,\mathbf{x}_A,\omega) \\
&\quad= -\frac{1}{\iota\omega} \int\limits_{S'} \frac{1}{\rho(\mathbf{x}')} \Bigg\{ \Bigg(\partial_{j'} \Bigg[-\frac{1}{\iota\omega} \int\limits_{S} \frac{1}{\rho(\mathbf{x})} \left[\left(\partial_j \hat{\check{G}}(\mathbf{x}',\mathbf{x},\omega)\right) \hat{\check{G}}^{*}(\mathbf{x}_B,\mathbf{x},\omega) \right. \\
&\quad\quad \left. - \hat{\check{G}}(\mathbf{x}',\mathbf{x},\omega) \left(\partial_j \hat{\check{G}}^{*}(\mathbf{x}_B,\mathbf{x},\omega)\right) \right] n_j \,\mathrm{d}S \Bigg] \Bigg) \hat{\check{G}}^{*}(\mathbf{x}',\mathbf{x}_A,\omega) \\
&\quad\quad - \Bigg[-\frac{1}{\iota\omega} \int\limits_{S} \frac{1}{\rho(\mathbf{x})} \left[\left(\partial_j \hat{\check{G}}(\mathbf{x}',\mathbf{x},\omega)\right) \hat{\check{G}}^{*}(\mathbf{x}_B,\mathbf{x},\omega) \right. \\
&\quad\quad \left. - \hat{\check{G}}(\mathbf{x}',\mathbf{x},\omega) \left(\partial_j \hat{\check{G}}^{*}(\mathbf{x}_B,\mathbf{x},\omega)\right) \right] n_j \,\mathrm{d}S \Bigg] \left(\partial_{j'} \hat{\check{G}}^{*}(\mathbf{x}',\mathbf{x}_A,\omega)\right) \Bigg\} n_{j'} \,\mathrm{d}S'
\end{aligned} \tag{2.43}$$

- Volume injection rate sources, Wapenaar & Fokkema (2006) approach, monopole sources

and receivers only:

$$\begin{aligned}&\hat{\hat{G}}(\mathbf{x}_B,\mathbf{x}_A,\omega)+\hat{\hat{G}}^{*}(\mathbf{x}_B,\mathbf{x}_A,\omega)\\&\qquad\approx\frac{2}{\rho c}\int\limits_{S'}\left[\frac{2}{\rho c}\int\limits_{S}\hat{\hat{G}}(\mathbf{x}',\mathbf{x},\omega)\hat{\hat{G}}^{*}(\mathbf{x}_B,\mathbf{x},\omega)\,\mathrm{d}S\right]\hat{\hat{G}}^{*}(\mathbf{x}',\mathbf{x}_A,\omega)\,\mathrm{d}S'\end{aligned}\tag{2.44}$$

- Volume injection rate sources, van Manen et al. (2005)-like approach, monopole and dipole sources and receivers:

$$\begin{aligned}&\breve{\hat{G}}(\mathbf{x}_B,\mathbf{x}_A,\omega)+\breve{\hat{G}}^{*}(\mathbf{x}_B,\mathbf{x}_A,\omega)\\&\quad=\frac{1}{\iota\omega}\int\limits_{S'}\frac{1}{\rho(\mathbf{x}')}\Bigg\{\Bigg(\partial_{j'}\Bigg[\frac{1}{\iota\omega}\int\limits_{S}\frac{1}{\rho(\mathbf{x})}\Big[\Big(\partial_j\breve{\hat{G}}(\mathbf{x}',\mathbf{x},\omega)\Big)\breve{\hat{G}}^{*}(\mathbf{x}_B,\mathbf{x},\omega)\\&\quad-\breve{\hat{G}}(\mathbf{x}',\mathbf{x},\omega)\Big(\partial_j\breve{\hat{G}}^{*}(\mathbf{x}_B,\mathbf{x},\omega)\Big)\Big]n_j\,\mathrm{d}S\Bigg]\Bigg)\breve{\hat{G}}^{*}(\mathbf{x}',\mathbf{x}_A,\omega)\\&\quad-\Bigg[\frac{1}{\iota\omega}\int\limits_{S}\frac{1}{\rho(\mathbf{x})}\Big[\Big(\partial_j\breve{\hat{G}}(\mathbf{x}',\mathbf{x},\omega)\Big)\breve{\hat{G}}^{*}(\mathbf{x}_B,\mathbf{x},\omega)\\&\quad-\breve{\hat{G}}(\mathbf{x}',\mathbf{x},\omega)\Big(\partial_j\breve{\hat{G}}^{*}(\mathbf{x}_B,\mathbf{x},\omega)\Big)\Big]n_j\,\mathrm{d}S\Bigg]\Big(\partial_{j'}\breve{\hat{G}}^{*}(\mathbf{x}',\mathbf{x}_A,\omega)\Big)\Bigg\}n_{j'}\,\mathrm{d}S'\end{aligned}\tag{2.45}$$

- Volume injection rate sources, van Manen et al. (2005)-like approach, monopole sources and receivers only:

$$\begin{aligned}&\breve{\hat{G}}(\mathbf{x}_B,\mathbf{x}_A,\omega)+\breve{\hat{G}}^{*}(\mathbf{x}_B,\mathbf{x}_A,\omega)\\&\qquad\approx-\frac{2}{\rho c}\int\limits_{S'}\left[-\frac{2}{\rho c}\int\limits_{S}\breve{\hat{G}}(\mathbf{x}',\mathbf{x},\omega)\breve{\hat{G}}^{*}(\mathbf{x}_B,\mathbf{x},\omega)\,\mathrm{d}S\right]\breve{\hat{G}}^{*}(\mathbf{x}',\mathbf{x}_A,\omega)\,\mathrm{d}S'\end{aligned}\tag{2.46}$$

2.5.1 Example 5 - Source-Receiver Interferometry in Frequency Domain

Run by executing the Matlab script `example_5__source_receiver_F.m`. With the given settings, the figures shown in Fig. 2.11, Fig. 2.12 and Fig. 2.13 are obtained. In this case, a positive volume injection source is used, and interferometry is performed in the frequency-domain using the formula in equation (2.40) (*N.B.*: in this example, the inter-source step of source-receiver interferometry uses only the causal part of the Green's function constructed from the first inter-receiver step, rather than the homogeneous Green's function (difference between the Green's function and its complex conjugate) as given in equation (2.40)). As indicated by the formula, the causal (positive-time) part of the interferometric Green's function matches the exact result modelled by placing a source at A and a receiver at B, while the acausal (negative-time) part of the interferometric Green's function matches the negative time-reverse of the true modelled result.

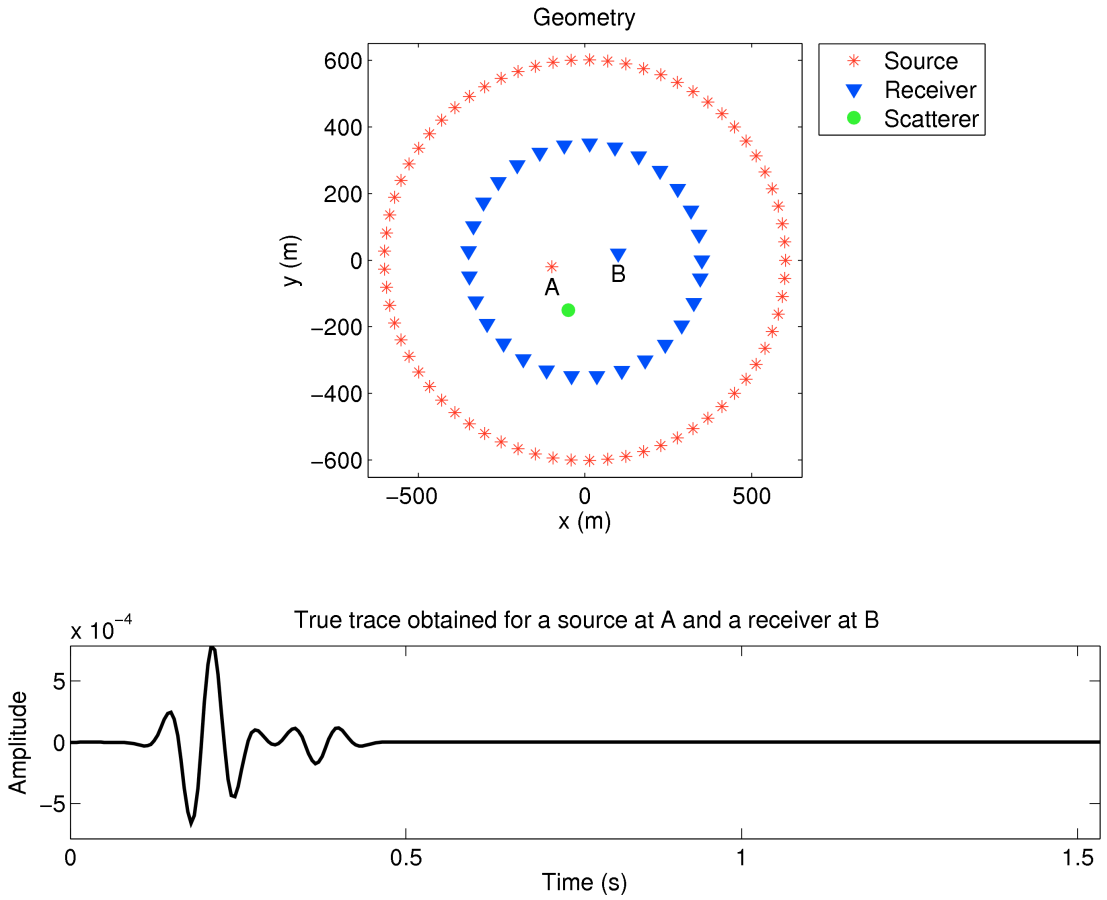

Figure 2.11. Geometry and true modelled trace in example 5. Only every fifth source and every seventh receiver are plotted for clarity.

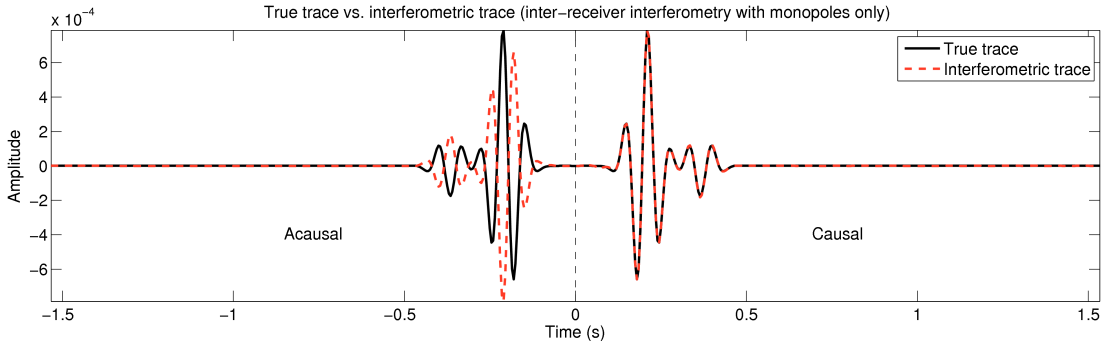

Figure 2.12. True trace and interferometric trace in example 5. When interferometry is performed using the formula in equation (2.40), the causal part of the interferometric trace matches the true trace, while the acausal part of the interferometric trace matches the negative time-reverse of the true trace.

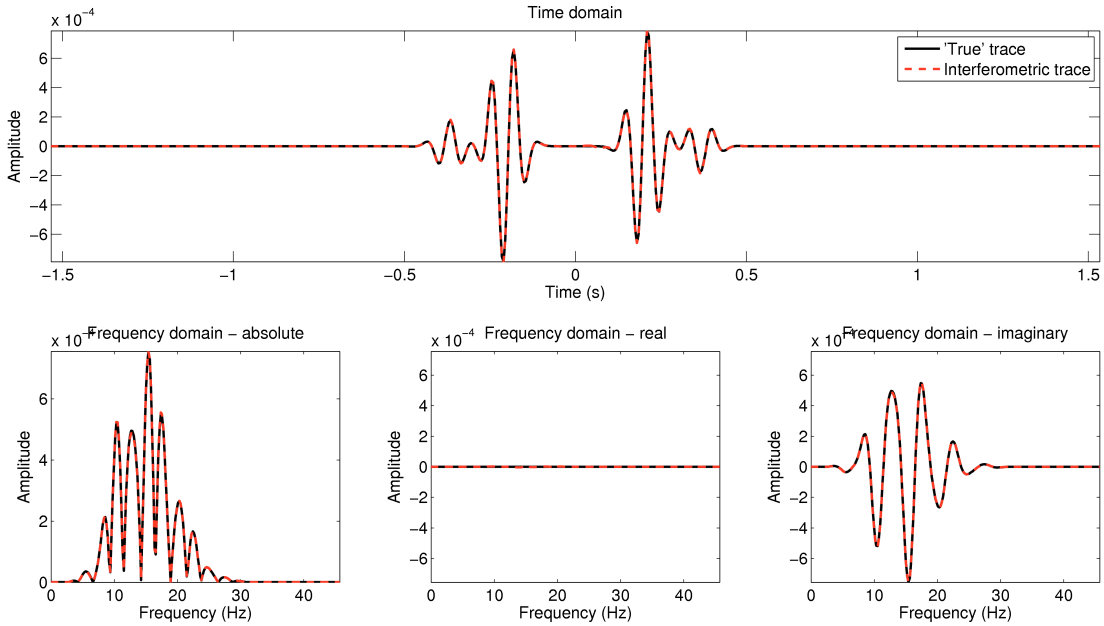

Figure 2.13. 'True' trace and interferometric trace in example 5. Top: the causal part of the 'true' trace is obtained by taking the true modelled trace in Fig. 2.11, while the acausal part is obtained by time-reversing the negative of true trace in Fig. 2.11, according to the formula in equation (2.40). Bottom left: frequency spectra. Bottom centre: real component of frequency - equal to zero when using the interferometric formula in equation (2.40). Bottom right: imaginary component of frequency.

2.6 Disclaimer

To the best of our knowledge this code is correct, error-free, and produces the results given in the examples above, as of March 2013 using the Linux version of Matlab 7.14.0 (R2012a). We can not guarantee its accuracy however. If after your own detailed investigation you believe there are errors in the code or worked examples, please contact Erica Galetti at `erica.galetti@ed.ac.uk` and/or Andrew Curtis at `Andrew.Curtis@ed.ac.uk`.

References

Curtis, A. & Halliday, D., 2010. Source-receiver wave field interferometry, *Physical Review E*, **81**(4), 046601.

Curtis, A., Gerstoft, P., Sato, H., Snieder, R., & Wapenaar, K., 2006. Seismic interferometry—turning noise into signal, *The Leading Edge*, **25**(9), 1082–1092.

Curtis, A., Nicolson, H., Halliday, D., Trampert, J., & Baptie, B., 2009. Virtual seismometers in the subsurface of the Earth from seismic interferometry, *Nature Geosci*, **2**(10), 700–704.

Douma, H., Vasconcelos, I., & Snieder, R., 2011. The reciprocity theorem for the scattered field is the progenitor of the generalized optical theorem, *The Journal of the Acoustical Society of America*, **129**(5), 2765–2771.

Foldy, L. L., 1945. The Multiple Scattering of Waves. I. General Theory of Isotropic Scattering by Randomly Distributed Scatterers, *Phys. Rev.*, **67**, 107–119.

Galetti, E. & Curtis, A., 2012. Generalised receiver functions and seismic interferometry, *Tectonophysics*, **532 - 535**(0), 1 – 26.

Galetti, E., Halliday, D., & Curtis, A., 2013. A simple and exact acoustic wavefield modelling code for data processing, imaging and interferometry applications, *Geophysics*, accepted.

Groenenboom, J. & Snieder, R., 1995. Attenuation, dispersion, and anisotropy by multiple scattering of transmitted waves through distributions of scatterers, *The Journal of the Acoustical Society of America*, **98**(6), 3482–3492.

Halliday, D. & Curtis, A., 2009. Generalized optical theorem for surface waves and layered media, *Physical Review E*, **79**(5), 056603.

MathWorks, 2012. Systems of Linear Equations, `http://www.mathworks.co.uk/help/matlab/math/systems-of-linear-equations.html`, Online - last accessed: 08 February 2013.

Minato, S., Matsuoka, T., Tsuji, T., Draganov, D., Hunziker, J., & Wapenaar, K., 2011. Seismic interferometry using multidimensional deconvolution and crosscorrelation for crosswell seismic reflection data without borehole sources, *Geophysics*, **76**(1), SA19–SA34.

Slob, E. & Wapenaar, K., 2007. Electromagnetic Green's functions retrieval by cross-correlation and cross-convolution in media with losses, *Geophys. Res. Lett.*, **34**(5), L05307.

Slob, E., Draganov, D., & Wapenaar, K., 2007. Interferometric electromagnetic Green's functions representations using propagation invariants, *Geophysical Journal International*, **169**(1), 60–80.

Snieder, R., 1999. *Diffuse waves in complex media*, vol. 531 of **NATO Science Series - Series C: Mathematical and Physical Sciences**, chap. Imaging and averaging in complex media, pp. 405–454, Kluwer Academic Publishers, Dordrecht, The Netherlands.

Snieder, R., 2009. *A Guided Tour of Mathematical Methods For the Physical Sciences*, Cambridge University Press, 2nd edn.

van Manen, D.-J., Robertsson, J. O. A., & Curtis, A., 2005. Modeling of Wave Propagation in Inhomogeneous Media, *Physical Review Letters*, **94**(16), 164301.

van Manen, D.-J., Curtis, A., & Robertsson, J. O. A., 2006. Interferometric modeling of wave propagation in inhomogeneous elastic media using time reversal and reciprocity, *Geophysics*, **71**(4), SI47–SI60.

Vasconcelos, I. & Snieder, R., 2008a. Interferometry by deconvolution: Part 1 – Theory for acoustic waves and numerical examples, *Geophysics*, **73**(3), S115–128.

Vasconcelos, I. & Snieder, R., 2008b. Interferometry by deconvolution: Part 2 – Theory for elastic waves and application to drill-bit seismic imaging, *Geophysics*, **73**(3), S129–141.

Wapenaar, K., 2004. Retrieving the Elastodynamic Green's Function of an Arbitrary Inhomogeneous Medium by Cross Correlation, *Physical Review Letters*, **93**(25), 254301.

Wapenaar, K. & Douma, H., 2012. A unified optical theorem for scalar and vectorial wave fields, *The Journal of the Acoustical Society of America*, **131**(5), 3611–3626.

Wapenaar, K. & Fokkema, J., 2006. Green's function representations for seismic interferometry, *Geophysics*, **71**(4), SI33–SI46.

Wapenaar, K. & van der Neut, J., 2010. A representation for Green's function retrieval by multidimensional deconvolution, *The Journal of the Acoustical Society of America*, **128**(6), EL366–EL371.

Wapenaar, K., van der Neut, J., & Ruigrok, E., 2008. Passive seismic interferometry by multidimensional deconvolution, *Geophysics*, **73**(6), A51–A56.

Wapenaar, K., Draganov, D., Snieder, R., Campman, X., & Verdel, A., 2010a. Tutorial on seismic interferometry: Part 1 – Basic principles and applications, *Geophysics*, **75**(5), 75A195–75A209.

Wapenaar, K., Slob, E., Snieder, R., & Curtis, A., 2010b. Tutorial on seismic interferometry: Part 2 – Underlying theory and new advances, *Geophysics*, **75**(5), 75A211–75A227.

Wapenaar, K., Ruigrok, E., van der Neut, J., & Draganov, D., 2011. Improved surface-wave retrieval from ambient seismic noise by multi-dimensional deconvolution, *Geophys. Res. Lett.*, **38**(1), L01313.

APPENDIX A

More Equations

A.1 Analytic Monopole and Dipole Green's Functions[1]

The monopole Green's function (impulse response) in a medium with constant velocity c satisfies the following equation in the frequency domain (the *Helmholtz equation*):

$$\nabla^2 G(\mathbf{x}, \mathbf{x}_0, \omega) + k^2 G(\mathbf{x}, \mathbf{x}_0, \omega) = -\delta(\mathbf{x} - \mathbf{x}_0) \ , \tag{A.1}$$

where $G(\mathbf{x}, \mathbf{x}_0, \omega)$ is the Green's function at location $\mathbf{x}$ due to a source at location $\mathbf{x}_0$, k is the wavenumber (which satisfies $k = \omega/c$, where ω is angular frequency), and the term $\delta(\mathbf{x} - \mathbf{x}_0)$ represents the source defined as a spatio-temporal impulse (delta function) acting at location $\mathbf{x}_0$ at time $t = 0$. The Helmholtz equation can be solved for the Green's function in N dimensions, and full derivations in one, two or three dimensions can be found in Snieder (2009). The solution to the Helmholtz equation is given in one dimension by

$$\begin{aligned} G^{1D}(x, x_0) &= -\frac{\iota}{2k} e^{-\iota k|x - x_0|} \\ &= -\frac{1}{2k} e^{-\iota\left(k|x - x_0| - \frac{\pi}{2}\right)} \ , \end{aligned} \tag{A.2}$$

in two dimensions by

$$G^{2D}(\mathbf{x}, \mathbf{x}_0) = -\frac{\iota}{4} H_0^{(2)}(k|\mathbf{x} - \mathbf{x}_0|) \ , \tag{A.3}$$

[1] This section is an (adapted) excerpt from Galetti et al. (2013).

in two dimensions (far-field case) by

$$\begin{aligned} G^{2D\text{-}far}(\mathbf{x},\mathbf{x}_0) &= -\frac{\iota}{4}e^{-\iota\left(k|\mathbf{x}-\mathbf{x}_0|-\frac{\pi}{4}\right)}\sqrt{\frac{2}{\pi k|\mathbf{x}-\mathbf{x}_0|}} \\ &= -\frac{1}{4}e^{-\iota\left(k|\mathbf{x}-\mathbf{x}_0|-\frac{3\pi}{4}\right)}\sqrt{\frac{2}{\pi k|\mathbf{x}-\mathbf{x}_0|}}\ , \end{aligned} \tag{A.4}$$

and in three dimensions by

$$G^{3D}(\mathbf{x},\mathbf{x}_0) = \frac{1}{4\pi}\frac{e^{-\iota k|\mathbf{x}-\mathbf{x}_0|}}{|\mathbf{x}-\mathbf{x}_0|}\ , \tag{A.5}$$

where $H_0^{(2)}$ is the Hankel function of the second kind and order 0, and the imaginary unit $\iota = \sqrt{-1}$ has been taken inside the exponential term in the second line of equations (A.2) and (A.4).

Dipole Green's functions may be obtained from spatial differentiation of equations (A.2)-(A.5) and are given by

$$\partial G^{1D}(x,x_0) = -\iota k G^{1D}(x,x_0) \tag{A.6}$$

in one dimension, by

$$\partial_m G^{2D}(\mathbf{x},\mathbf{x}_0) = \frac{\iota k}{4}\cos(\phi_m)H_1^{(2)}(k|\mathbf{x}-\mathbf{x}_0|)\ , \tag{A.7}$$

in two dimensions, by

$$\partial_m G^{2D\text{-}far}(\mathbf{x},\mathbf{x}_0) = -G^{2D\text{-}far}(\mathbf{x},\mathbf{x}_0)\cos(\phi_m)\left[\iota k + \frac{1}{2|\mathbf{x}-\mathbf{x}_0|}\right]\ , \tag{A.8}$$

in two dimensions (far-field case), and by

$$\partial_m G^{3D}(\mathbf{x},\mathbf{x}_0) = -G^{3D}(\mathbf{x},\mathbf{x}_0)\cos(\phi_m)\left[\iota k + \frac{1}{|\mathbf{x}-\mathbf{x}_0|}\right]\ , \tag{A.9}$$

in three dimensions. $H_1^{(2)}$ is the Hankel function of the second kind and order 1, and the term $\cos(\phi_m)$ is the direction cosine of the receiver position $\mathbf{x}$ with respect to the source location $\mathbf{x}_0$ along the m-direction, i.e., the cosine of the angle between vector $\mathbf{x}-\mathbf{x}_0$ and the m-direction. Note that the above equations assume the exponential term in the Fourier transform from frequency to time domain to be $e^{\iota\omega t}$, which is the sign convention used by Matlab (as opposed to $e^{-\iota\omega t}$, which is more usual in Geophysics, for example).

A.2 Scattering Amplitude in D-Dimensions[2]

For a certain distribution of N isotropic point scatterers, the scattering amplitude $A^{(i)}$ of scatterer (i) located at $\mathbf{x}^{(i)}$ is a complex quantity that relates the total wavefield $\Psi_0(\mathbf{x}^{(i)})$ incident on the scatterer to the scattered wavefield $\Psi_S(\mathbf{x})$ measured at $\mathbf{x}$, according to

$$\Psi_S(\mathbf{x}) = \Psi_0(\mathbf{x}^{(i)}) A^{(i)} G(\mathbf{x}, \mathbf{x}^{(i)}) \ , \tag{A.10}$$

where $G(\mathbf{x}, \mathbf{x}^{(i)})$ is the Green's function between $\mathbf{x}^{(i)}$ and $\mathbf{x}$. As shown by Snieder (1999), the scattering amplitude contains the superposition of all possible multiple scattering interactions with the same scatterer and, since scattering is assumed to be isotropic, is independent of the angle of incidence.

The real and imaginary parts of the scattering amplitude are related via the optical theorem (generally, an optical theorem describes the conservation of energy between a wave incident on a scattering object and the resulting wave scattered by that object). In simple acoustic media with uniform background velocity, the relationship between the real and imaginary part of the scattering amplitude can be derived by equating the total energy loss for unit incident wavefield (the so-called *total cross-section* Ω_T) to the total scattered energy (the so-called *scattering cross-section* Ω_S). This approach assumes that no energy is lost to anelastic attenuation, hence the energy loss of the incident wavefield is due to scattering alone.

In two dimensions, the total and scattering cross-sections are given respectively by (Groenenboom & Snieder, 1995)

$$\Omega_T = -\frac{\Im(A)}{k} \tag{A.11}$$

and

$$\Omega_S = \frac{|A|^2}{4k} \ , \tag{A.12}$$

where the latter expression is obtained by using the far-field Green's function (equation A.4) to get Ψ_S in equation A.10 and integrating the power of the scattered field $|\Psi_S|^2 = \Psi_S \Psi_S^*$ over 2π. Using a similar approach, expressions similar to those in the above equations can be derived in one and three dimensions, and by equating the total and scattering cross-sections the relationships between the real and imaginary parts of the scattering amplitude can be obtained in one, two and three dimensions (Snieder, 1999):

$$\Re(A) = \pm \begin{cases} \left(-\Im(A)\left[2k + \Im(A)\right]\right)^{1/2} & \text{in 1D} \\ \left(-\Im(A)\left[4 + \Im(A)\right]\right)^{1/2} & \text{in 2D} \\ \left(-\Im(A)\left[\dfrac{4\pi}{k} + \Im(A)\right]\right)^{1/2} & \text{in 3D} \end{cases} \tag{A.13}$$

These expressions impose the following constraints on the value of the imaginary part of the

[2]This section is an (adapted) excerpt from Galetti et al. (2013).

scattering amplitude:

$$\begin{aligned} -2k \leq \Im(A) \leq 0 \quad & \text{in 1D} \\ -4 \leq \Im(A) \leq 0 \quad & \text{in 2D} \\ -\frac{4\pi}{k} \leq \Im(A) \leq 0 \quad & \text{in 3D} \end{aligned} \tag{A.14}$$

The relationships between the real and imaginary components of A are of particular importance as they ensure that the scattering strength of each scatterer satisfies the requirement of energy conservation. Optical theorems for more complex scattering media also exist (Halliday & Curtis, 2009; Douma et al., 2011; Wapenaar & Douma, 2012) and can be applied to obtain a correct estimate of the scattering amplitude. However, the details of these theorems will not be discussed here as their application is beyond the scope of our simple modelling code.

A.3 A Note on Source Types

Because of the different sign conventions used by Wapenaar & Fokkema (2006) and van Manen et al. (2005), the following relationships arise between the Green's functions listed in section A.1 and those used in interferometry (section 2.2):

$$\hat{G} = G \tag{A.15}$$

$$\hat{\hat{G}} = \iota\omega G \tag{A.16}$$

$$\check{G} = -G \tag{A.17}$$

$$\check{\check{G}} = -\iota\omega G \tag{A.18}$$

where G can denote either the one-, two-, or three-dimensional Green's function as in equations (A.2)-(A.5), and the same hat symbol convention as in section 2.2 is used to denote the interferometric Green's functions.